Scientific progress of the MC-PAD network

(Period P1: November 2008 – October 2010)

November 2010

The MC-PAD network

MC-PAD is a multi-site Initial Training Network on particle detectors in physics experiments. It comprises nine academic participants, three industrial partners and two associated academic partners. Today, 17 recruited Early Stage and 4 Experienced Researchers are performing their scientific work in the network.

The research and development work of MC-PAD is organized in 12 work packages, which focus on a large variety of aspects of particle detector development, electronics as well as simulation and modelling.

This report was produced on the occasion of the project's midterm review. It summarizes the scientific progress and highlights the main achievements.

Table of contents

Project 1: Radiation Tolerant Mini-strip Tracking Detectors

Project Coordinator: Michael Moll, CERN.

Nicola Pacifico, ESR, CERN. Supervisor: Michael. Moll.

Tomas Balog, ESR, GSI. Supervisor: Johann Heuser.

Two ESR's, based at CERN and GSI, are working in the framework of project P1 on the development of radiation tolerant silicon detectors for High Energy Physics. The ESR at CERN started in January 2009, while the project at GSI could only effectively start in July 2010 with the hiring of a replacement for the first ESR, who unfortunately left the MC-PAD network after a few months.

Activities of the ESR at CERN

The main focus of the activities at CERN during the first 18 months has been addressed towards the development of new instruments and techniques for the study of radiation damage on strip sensors. The ESR participated in the construction of a new CV/IV setup with a cold chuck and essentially built two new setups by himself:

- A Charge Collection Efficiency (CCE) measurement setup for microstrip detectors which allows the direct study of the Signal to Noise Ratio (SNR) performance of a strip detector. It is based on the ALIBAVA readout system, which uses the LHCb Beetle readout chip. Irradiated detectors can be investigated in typical operational conditions (low temperature and humidity). A beta source or an infrared laser is used to induce a signal charge simulating the particle flux in the high energy physics experiments.
- An Edge-TCT (Transient Charge Technique) setup which allows by means of a highly focused infrared laser to investigate the charge carrier drift velocity and the electric field strength as function of depth in the detector. This data is most valuable when complemented with data obtained from microscopic defect studies (e.g. TSC or DLTS measurements). Furthermore, it is a perfect tool to study avalanche effects in ministrip sensors which have recently been identified to be one of the key elements in explaining the improved radiation tolerance of highly irradiated p-type silicon sensors. The analysis of the data obtained with this technique and the corresponding software analyses tools pose a major challenge and are present research activities followed up by the ESR.

In parallel to the above described activities, the ESR conducted several measurements on different kind of detectors. A study on low resistivity Magnetic Czochralski (MCz) silicon showed that this kind of material has remarkable radiation hardness with performances that are under particular conditions comparable to those of p-type silicon detectors, without however posing the engineering challenges typical of n-implant readout detectors. The study has been presented by the ESR at the RESMDD10 conference and will be published in the conference proceedings. An example of the analyses of an Edge-TCT measurement is given in Figure 1.

In summer 2010 the ESR supervised a summer student project on the annealing of the charge collection efficiency of standard Hamamatsu FZ p-on-n detectors which are used in the present generation of LHC experiments. The aim of the project was to gain a better understanding of the

performance degradation to be expected in long term operation and the impact of unexpected failures of the cooling systems in the LHC experiments. The outcome of the study will be presented at the 17th RD50 workshop in November 2010.
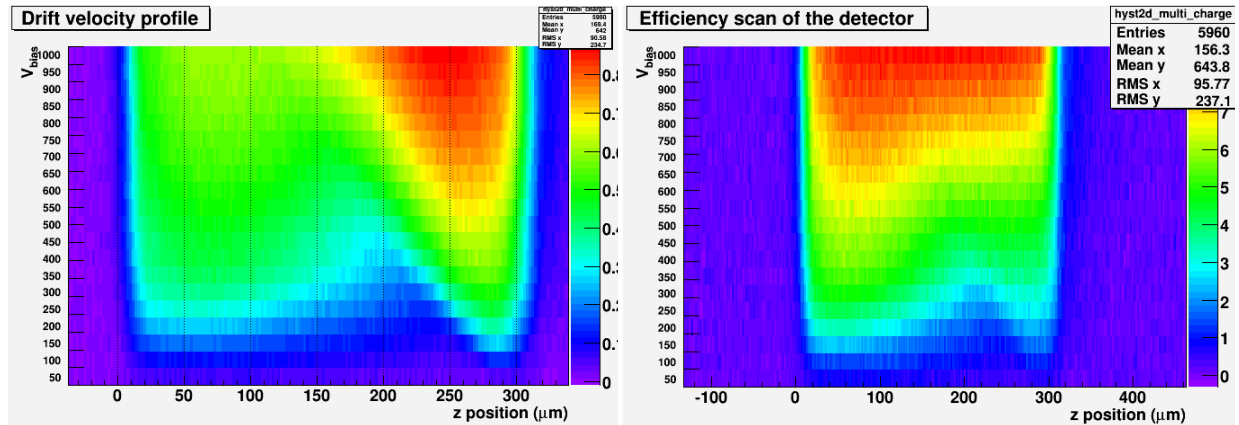

Figure 1: Drift velocity and charge collection efficiency (CCE) depth profiles for a MCz p-on-n low resistivity silicon detector irradiated with 3×10^{15}n/cm^2. It can be seen that the charge carrier drift velocity profile and the CCE as function of depth inside the detector are not directly correlated. The effect is probably due to a higher trapping of holes with respect to electrons.

All the setups mentioned above are currently used for the testing of prototype sensors for the LHC upgrade. The main activity is performed in the context of an international research and development program of several institutes aiming to define the detector material and concept for the forthcoming upgrade of the CMS silicon tracker system. A key element of this collaborative effort is the exchange and share of data between the involved institutes. For this reason, extensive preparation work has been addressed to the cross-calibration of measurement setups in the various institutes and the development of a dataflow system allowing to share all measurements in a common database. Up to now, CV/IV and Edge-TCT measurements have been performed on a set of detectors for the pre-irradiation characterization. Irradiation of the detectors is presently ongoing and characterization of detectors after irradiation and in dedicated annealing experiments will soon start.

Activities of the ESR at GSI

The work started in June 2010 and in a first phase focussed on the study and the simulation of the self-triggered n-XYTER frontend chip which has been developed for neutron physics experiments and is used in this project for the early prototyping of CBM detectors [1]. Aim of the simulation is to understand if the high data rates in the CBM experiment can lead to overload situations in the chip which, without further measures, could lead to uncontrolled data losses. Based on the outcome of the simulations, possible modifications of the chip architecture to control data losses and allow for software definitions of dead time will be investigated.

The simulations are performed using the hardware description language SystemC which is built on C++ standard extended with class libraries and a runtime system [2]. SystemC addresses the need for a system design and verification language that spans hardware and software.
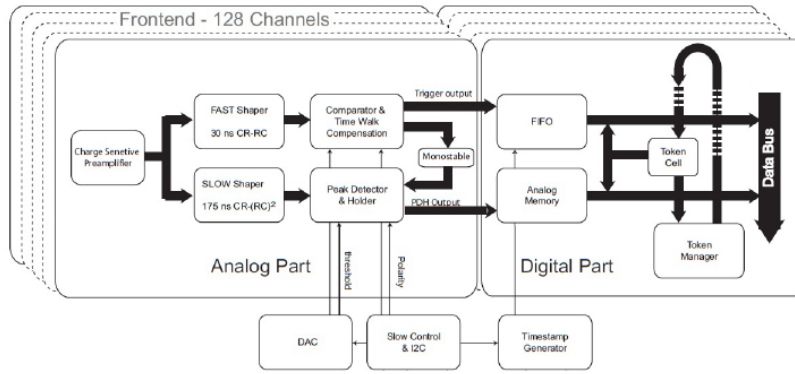
Fig. 2: Structure of n-XYTER electronics [3].

The schematic structure of n-XYTER chip is shown in Fig.2. In order to simplify the simulation the fast and slow shapers were removed and for all the modules after the Token Ring it was assumed that no data loss occurred. The modules comprised in the simulation are the FIFOs with a depth of 4 cells and the Token Ring. In addition there is a data generator which generates time periods for next incoming data and also makes decisions in which FIFO data has to be written. The selection of the FIFO is made according to Uniform distribution. The period of data reading by the Token Ring is 32ns for every n-XYTER chip. The Token Ring is able to read data only from one FIFO in one period. In case of every FIFO being filled with at least one data entry the reading period for each FIFO is approximately 4µs.
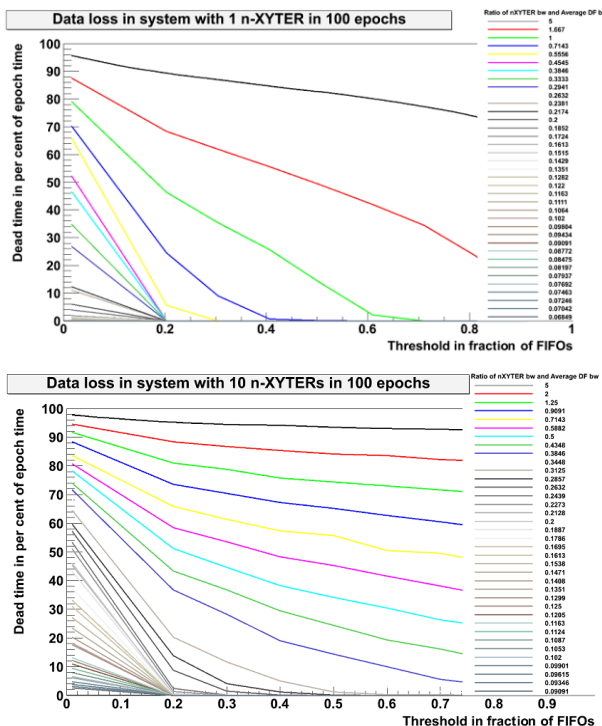

Fig. 3: Comparison of results for 1 and 10 n-XYTER chips with respect to keeping the same bandwidth of incoming data for all chips and to ratios of the Token Ring bandwidth and average data flow bandwidth.

To introduce controlled data losses a counting module has been added. Every channel has its own counter which increments by one with incoming data in the FIFO. In case of reaching four counts (number of counts has to agree with depth of the FIFO) the particular FIFO is closed. All FIFOs are again opened and counters are set to zero after the epoch period has elapsed. An epoch period is defined as the time needed for reading all cells from all FIFOs in one chip by the Token Ring. This corresponds to approximately 16µs.

The beginning of the dead time is the moment when the number of the closed FIFOs reaches a predefined value. The dead time is later expressed in per cent of the epoch time. The results of a simulation of the behaviour of a system with one n-XYTER chip compared to systems of 10 n-XYTER chips is shown in Fig.3.

From shown results we can see that the dead time is increasing with the system size which reflects the increasing probability of filling up more n-XYTER chips in shorter time. As a consequence, with the average bandwidth of incoming data for each n-XYTER kept constant in larger systems, the dead time of the system increases with the size of the system. The determination of the optimum system size is one of the aims of forthcoming simulations.

References:

[1] C.J. Schmidt et al.: Characterization of the n-XYTER chip and preparations for the engineering run, CBM Progress Report 2009, http://www-cbm.gsi.de

[2] http://www.systemc.org

[3] A.S.Brogna et al.: The n-XYTER reference manual, 2009

Project 2: Hybrid Pixel Detectors

Project Coordinator : Tilman Rohe, PSI

Jennifer Sibille, ESR, PSI. Supervisor: Tilman Rohe.

Jiaguo Zhang, ESR, UHH. Supervisor: Robert Klanner.

1 Introduction

The performance of the presently installed pixel detectors closest to the LHC beam will degrade considerably after a few years due to radiation damage. Also the newly developed X-ray sources, in particular the European X-FEL, pose unprecedented requirements in terms of radiation hardness and instantaneous photon densities.

The project aims for an understanding of the suitability and the limits of pixel detectors built with cost effective "standard" components. The target applications are the phase I upgrade of the CERN-CMS pixel detector and the AGIPD instrument for the European X-FEL in Hamburg. As the requirements of these projects are quite different, the project is presented in two parts.

2 R&D for a Photon Detector

The investigations are done by ESR Jiaguo Zhang at University of Hamburg.

Photons affect mainly the surface region of silicon detectors, which is the interface between the silicon bulk and the covering SiO_2.

2.1 Extraction of fixed oxide charge density and interface trap density

The two parameters mainly affected by photon irradiation are the density of fixed oxide charge and the concentration of interface traps. In a first step special test structures were investigated to experimentally determine the changes of these parameters with dose. The irradiation were done at a special irradiation facility at beamline F4 at the HASYLAB DORIS III synchrotron. This facility was set-up and is operated by the Hamburg group.
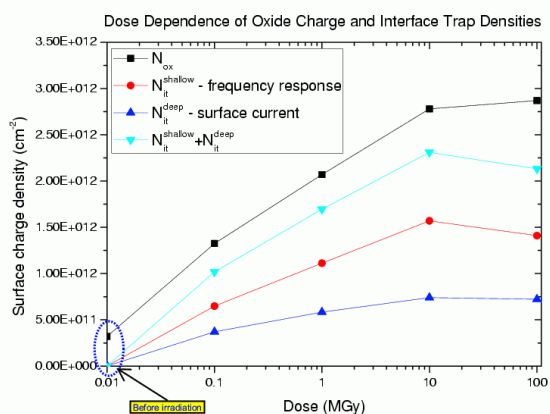

Figure 1: Measured dose dependence of surface properties.

MOS capacitors and gate-controlled diodes were irradiated with 100 kGy, 1 MGy, 10 MGy and 100 MGy doses with X-rays of ~ 12 keV. All test structures were annealed at 80°C for 60 minutes before the measurements, in order to stabilize the electric properties. CV (MOS-capacitance vs. voltage), IV (leakage current as function of the applies voltage) and TSC (Thermally Stimulated Current) measurements were performed. The interface trap densities were derived from the TSC spectrum; the oxide charge densities were obtained from the shift of the flatband voltages of the CV curves after subtracting the charge densities of the interface traps, and surface recombination velocities were determined directly from the IV curves of gate-controlled diodes. It was found that both oxide charge density and interface trap density saturate (or even decrease) for doses above ~1MGy.

The microscopic parameters, oxide charge density and interface trap density, were extracted as function of dose and were used as input parameters for a Synopsys TCAD simulation with the aim to describe the measurements on the test structures and to predict and optimize the sensor performances [ZHANG 2010].

2.2 Irradiation and characterization of segmented sensors

In order to optimize the design of radiation hard silicon pixel sensors for the AGIPD, the performance of X-ray irradiated segmented silicon sensor has to be understood on the basis of the parameters extracted in 2.1. Different types of segmented sensors, p^+ on n microstrip sensors and n^+ on n pixel sensors, were irradiated up to 10 MGy and the sensors' electric properties were characterized for different doses.

For a p^+ on n microstrip sensor, which has been irradiated without applied bias voltage, total capacitance, dark current and interstrip capacitance were measured as function of bias voltage. Photon irradiation leads to an increase of the full depletion voltage of the microstrip sensor by ~10V which saturates for higher doses visible in the CV-curve shown in Fig 2 (b). This can be explained by electrons accumulating at the Si-SiO$_2$ interface between the strips, which is caused by radiation induced positive oxide charges. The accumulated electrons delay the increase of the depleted volume, which leads to an increase of the full depletion voltage. For surface charge densities below 10^{11} cm^{-2} the full depletion voltage of microstrip sensors depends on the surface charge density; for values above ~10^{11} cm^{-2} it does not change any more [ZHANG 2010].

The dark current of irradiated sensors shows an almost linear increase with bias voltage. Even above full depletion, no saturation is observed as shown in Fig. 2 (a). This linear increase can be explained by the interface traps and the electron accumulation layer at the surface of the interstrip region. Only the interface traps in the region exposed to an electric field contribute to the measured dark current. At low bias voltages this interface region is "covered" by the electron accumulation layer and does not contribute to the leakage current. With increasing bias voltage the electron accumulation layer reduces (also above full depletion), and the surface exposed to the electric field and thus the surface current increases. The electron accumulation layer acts as a conductor, which explains the decrease of the interstrip capacitance with bias voltage.

As a next step a p^+ on n microstrip sensor was irradiated to ~1 MGy dose with ~35 V bias voltage applied. The data were compared to those taken with a sensor irradiated without bias being applied. It was found that there were no differences in the total capacitance, but there were differences in the dark current and the interstrip capacitance. Compared to the irradiation without bias voltage,

the increased dark current and the increased interstrip capacitance indicate that more surface charges were generated due to the presence of electric field during irradiation. This is expected as the field reduces the recombination probability of electrons with holes.
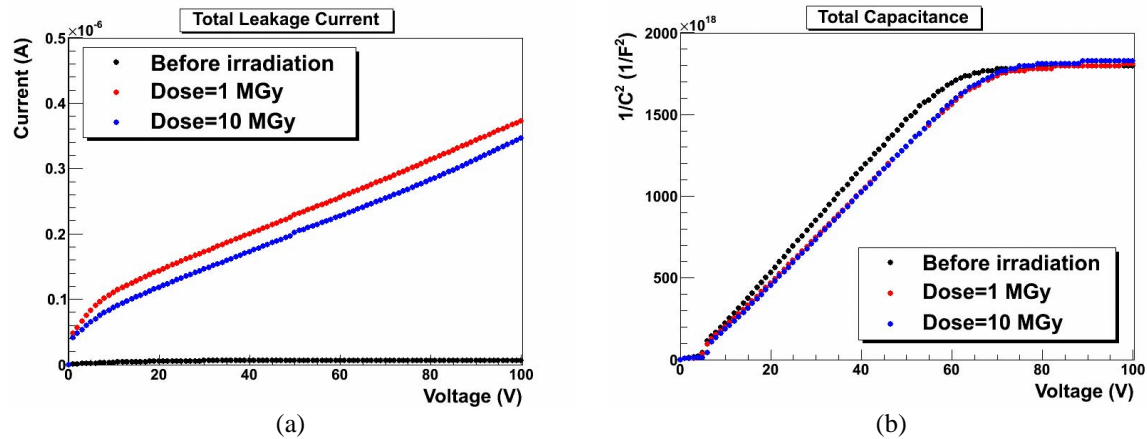
Figure 2: Change of the leakage current (a) and the full depletion voltage (b) caused by photon irradiation (without applied sensor bias).

The performance of a n$^+$ on n pixel sensor was also characterized for similar X-ray doses as mentioned above. In contrast to the p$^+$ on n microstrip sensor, no change of the full depletion voltage was observed after irradiation. This can be explained by the presence of a p-spray isolation implantation below the Si-SiO$_2$ interface in the inter-pixel region. The fixed oxide charge therefore caused a depletion layer in the p-spray below the surface and no electron accumulation. The dark current of those pixel sensors also showed a linear increase with bias voltage which is not fully understood yet, but is probably due to surface current from the region between the guard rings and the active sensor region.

2.3 Design of sensor and test structures

The specifications of the sensors for the AGIPD for the European XFEL have been finalized. The design of test structures, like pad diodes, gate controlled diodes, MOS capacitors, baby sensor and of the complete sensor has started using the commercial layout editor Cadence Virtuoso.

3 R&D for applications in Particle Physics

The investigations are done by ESR Jennifer Sibille at PSI.

At the LHC, pixel detectors are exposed to large doses of radiation which degrade the performance over time. The aim of this project is to develop hybrid pixel detector designs which can withstand these radiation doses, using standard components. One of the key steps in this process is to first understand the operational limits of currently existing sensors by examining how their characteristics are affected by radiation damage.
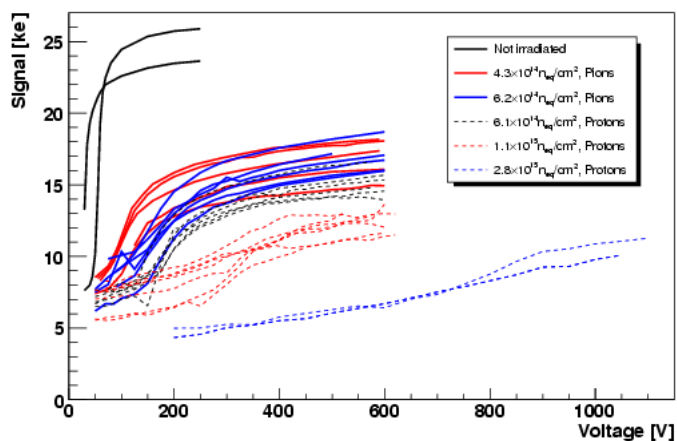
9

Figure 3: Signal charge induced by a Sr-90 source as a function of the sensor bias for irradiated sensors.

3.1 Charge Collection Efficiency

One of the key effects of radiation damage to the silicon sensors is a reduction in charge collection efficiency. Charges are trapped in defects in the silicon, and so a higher bias voltage must be applied, and a lower signal is seen. When the signal is too low to be detected by the read-out electronics, the detection efficiency is reduced.

Sensors from the production run of the CMS barrel pixel detector, already bump-bonded to read-out chips, were irradiated to various fluences, with 300 MeV positive pions at PSI up to 6.2×10^{14} n_{eq}/cm^2, and with 21 GeV protons at CERN up to 5.1×10^{15} n_{eq}/cm^2. The samples were tested at a temperature below -10 °C using a Sr-90 source. The signal obtained from the samples as function of the sensor bias is shown in Fig. 3. A substantial signal was seen even at high fluences, provided a high enough bias voltage was applied. For the highest fluences, no saturation of the signal charge was seen. The connectors limited the capability to reliably apply bias voltages higher than 600 V. For the samples at to 2.8×10^{15} n_{eq}/cm^2 it was possible to apply a bias voltage up to 1000 V, and a signal of 10 000 electrons was seen [SIBILLE 2010]. The samples were destroyed after being tested at 1000 V by sparking on the PCB.

3.2 Inter-pixel Capacitance

The inter-pixel capacitance is related to several characteristics of the detector, specifically the noise, cross talk, and time walk. The capacitance is inversely proportional to the spacing between pixel implants, called the gap. Therefore in designing a pixel sensor there is a trade off between minimizing the capacitance and minimizing the gap size. Measurements and simulations are in process to investigate how the capacitance changes with gap size, irradiation, and bias voltage.

A new method for measuring the inter-pixel capacitance has been developed. A read-out replacement chip has been designed and bump-bonded onto the sensors to be tested. This chip allows the measurement of the capacitance of a pixel with respect to its 8 neighbour pixels. The capacitance of several samples was measured. The samples included sensors from the production run of the current CMS barrel pixel detector, which have a gap of 20μm, and sensors with a gap of 30μm. Some of the sensors of each design were irradiated using a Co-60 source to a dose of 20kGy.

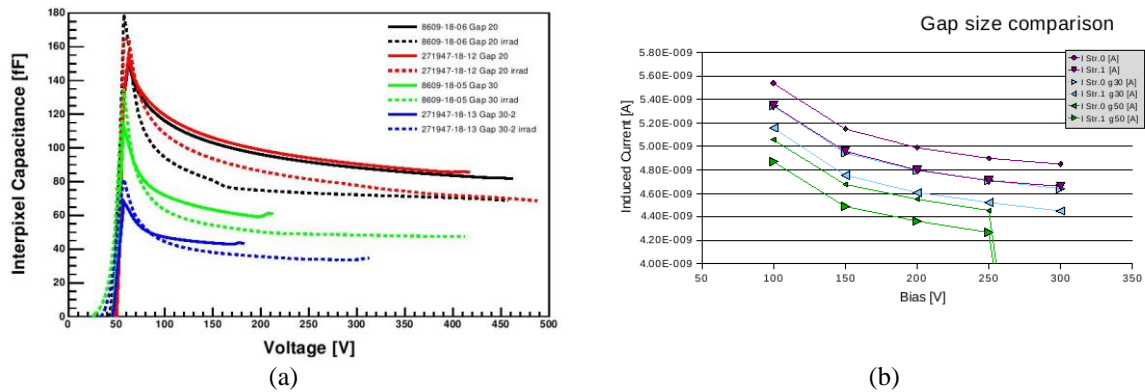(a)   (b)

Figure 4: Comparison of the measured interpixel capacitance before and after irradiation with 20kGy photons from a Co-60 source for two different gap sizes (a) . TCAD simulation (b) of the total pixel capacitance (Str.0) and the capacitance to the next neighbour (Str.1). The current shown in the Y-axis is proportional to the capacitance, however the conversion factor is not, yet, known.

The measurements confirm that a larger gap size leads to a smaller inter-pixel capacitance as shown in Fig 4 (a). The capacitance decreases with an increase in bias voltage. A possible explanation is that the p-spray isolation between the pixels is being depleted. It was also found that after irradiation the capacitance decreases. TCAD simulations were performed using a simplified 2-dimensional geometry, with only the pixels immediately to the right and left of the pixel being measured. The trend of the simulation results shown in Fig. 4 (b) follows the same trend as that seen in the measurements, however scaling between the simulations and measurements is still under work, so an absolute comparison can not be made yet.

3.3 Single-sided sensors

Aside from the bump-bonding of the sensors to the read-out chips, the most expensive part of the pixel detector are the sensors. The sensors used currently in the LHC detectors are made with a double-sided process. This allows the use of guard rings on the back side of the detector to bring the sensor edges to ground potential. A single-sided process gives a factor of 2-3 reduction in cost but leaves the sensor edges at high voltage, which creates a risk of sparking between the read-out chip and the sensor. Therefore a single-sided process is only feasible if a cheap and reliable solution to the sparking problem can be found.

Several single-sided sensors were obtained from the PSI-PILATUS group to use as test structures. The sensor bias was slowly increased until a discharge occurred. The discharge was seen by a spike in the current, and was also clearly audible in the testing lab. Three samples were tested and found to have a breakdown voltage between 550 V and 650 V. The discharge destroyed the samples. The damage on the

Figure 5: Photograph of a burned wire bond pad. The metallization of the sensor back side is also damaged

readout chip's ground pad and on the sensor back side is clearly visible (see Fig 5). Some sensors

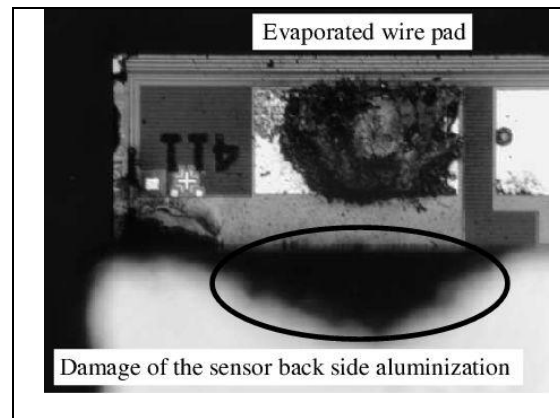were coated with a glue along the edges to attempt to prevent the breakdown. Two different glues were tried, Araldit and EPO-TEK 301, without any significant change to the breakdown voltage. There are plans to try another glue (EPO-TEK 302), as well as a thin edge passivation using chemical vapor deposited polymer.

References

[ZHANG 2010]   A. Srivastava, E. Fretwurst, R. Klanner, I. Pintilie, **J. Zhang**: Developement of radiation hard Si pixel sensors for the 4th generation photon science, Internal Note http://mc-pad.web.cern.ch/mc%2Dpad/SiPixel_for_XFEL.pdf

[SIBILLE 2010]   T. Rohe, J. Acosta, A. Bean, S. Dambach, W. Erdmann, U. Langenegger, C. Martin, B. Meier, V. Radicci, **J. Sibille**, P. Trüb: Signal height in silicon pixel detectors irradiated with pions and protons, NIM A 612 (2010) 493-496

Project 3: Radiation Hard Crystals/3D Detectors

Project Coordinator: Robert Klanner, University Hamburg

Marko Milovanović, ESR, Jozef Stefan Institute, Ljubljana,. Supervisor: Gregor Kramberger

Cristina Pirvutoiu, ESR, University of Hamburg. Supervisor: Robert Klanner,

Introduction

The radiation damage is the main limitation for the operation of position sensitive silicon detectors at future high energy physics experiments. At the time of the MC-PAD proposal, P3 focused on studies of radiation harder silicon crystals (epitaxial silicon) and so called 3D detectors. In 3D detectors the electrodes are not on the surface of the detector (planar) but inside the bulk of the detector perpendicular to the surface. The advantage of such a structure is that the number of charges created by a traversing particle is given by the thickness, while the drift length of the charges and the maximum depletion depth is given by the inter-electrode spacing. In this way two main negative effects of radiation damage, the increase of the space charge and thus of the depletion voltage, and the decrease of the signal due to the trapping of the drift length can be optimized separately and larger signals can be obtained than for a planar detector of the same thickness. However, 3D detectors also have drawbacks (higher electrode capacitance, regions of low electric field, and a complex and not yet mature technology).

It was expected, that the signal from planar silicon detectors would degrade with irradiation to a level where the efficient operation of the innermost tracking detectors at the SLHC would become impossible. However, recent measurements with planar detectors using n^+ readout electrodes (n^+-p or n^+-n detectors) showed a charge collection efficiency (CCE, CCE=1 for a fully depleted un-irradiated sensor) sufficient for the efficient operation even at the highest fluences expected at the SLHC of $1.6 \cdot 10^{16}$ hadrons cm^{-2}. The key condition was the operation at bias voltages around 1000 V. Several groups reported CCE much larger than expected, in some operating conditions even exceeding CCE=1. This is a clear evidence for charge multiplication. Charge multiplication was also reported for 3D detectors.

As charge multiplication may well be the solution for the operation of heavily irradiated silicon detectors, we decided to focus our studies on this phenomenon and concentrated our efforts on understanding the device model and operation of heavily irradiated planar silicon detectors. Both standard and epitaxial detectors were investigated.
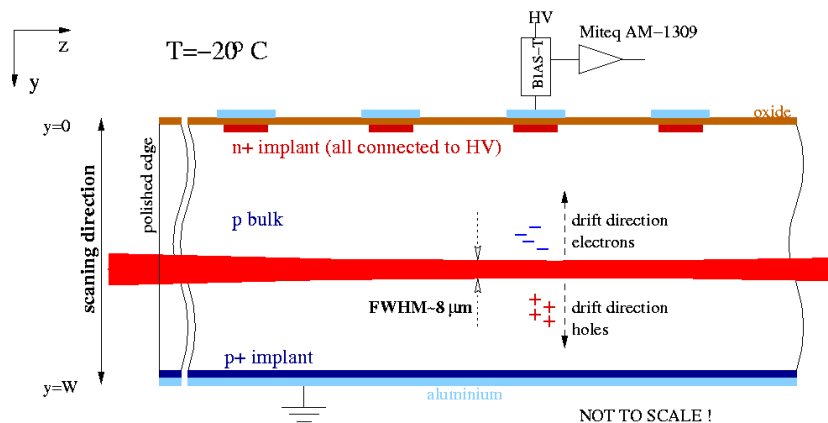
Charge collection and charge multiplication studies

For the detailed experimental study of the properties of silicon detectors as function of dose and type of irradiation, two complementary TCT-setups (Transient Current Technique) were developed and built in Hamburg and Ljubljana:

- m-TCT-setup (multi-channel-TCT) in Hamburg,
- edge-TCT-setup in Ljubljana.

Another setup utilizing a preamplifier followed by 25 ns shaping amplifier was also used to measure signals in epitaxial detectors with minimum ionizing electrons from a ^{90}Sr source.

In the Transient Current Technique electron-hole pairs are created near the surface of the detector by a short pulse (~100 ps) of visible light with small penetration depth or by alpha particles. In the electric field one type of charge carriers promptly reaches the neighboring electrode, while the carriers of the other type drift to the opposite electrode and induce a current which depends on their drift velocity. The current is measured by a wide band current amplifier and recorded by an oscilloscope (for m-TCT for several electrodes). From the time resolved current pulses the drift velocity of the charge carriers and the charge collection properties are obtained. The TCT-setup can also be used with IR light of large penetration depth where the e-h pairs are created with a spatial distribution similar to that of minimum ionizing particles. After irradiation to very high fluences the charges are quickly trapped, the induced current pulse is reduced and cannot be distinguished from the noise. This limits the use of TCT for the extraction of drift velocity and electric field profiles.

In the framework of MC-PAD/P3 a new technique, called Edge-TCT (see Fig. 1), was developed, which overcomes this difficulty. A focused laser beam of infrared light (λ=1060 nm, 100 ps pulse, 200 Hz repetition rate) illuminates the carefully polished edge of the detector. The electron-hole pairs are created almost uniformly along the beam. The beam position and thus the depth at which the carriers are created can be controlled by moving stages with sub-micron precision. The beam scan in the direction perpendicular to the surface (y-axis) reveals the charge collection efficiency for a given depth in the detector. At the beginning of the pulse the current is not yet affected by trapping and thus proportional to the drift velocity of the carriers and a model independent extraction of the velocity profile is possible. Moreover, the induced charge at a given depth reveals regions of high/low charge collection efficiency in the detector.

Figure 1: Shematic view of the Edge-TCT.

The measurement of the induced currents also gave a first direct observation of charge multiplication as can be seen in Fig. 2. After the initial peak, which is due to the drift of the primary generated carriers, a second peak appears at a time which depends on the position of the beam. This peak is due to electrons which reach the high field region close to the strips where they are multiplied. The holes produced in the multiplication process drift away from the strips and give rise to the second peak. The velocity profiles, shown in Fig. 3, also demonstrate that at high fluences a substantial electric field is present in the entire depth of the detector.

In the last year systematic studies have been made with the Edge-TCT on silicon strip detectors produced by Micron and HPK irradiated up to fluences of Φ_{eq}=1·10^{16} cm^{-2}. The most important observations are:
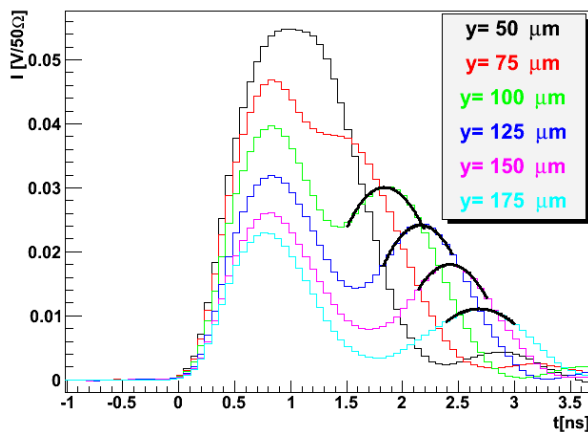
Figure 2: Induced current pulses for different depths of laser beam in a FZ n+-p strip detector irradiated by reactor neutrons to Φeq=5·1015 cm-2. The detector was annealed for 80min at 60°C and biased to 1000V.
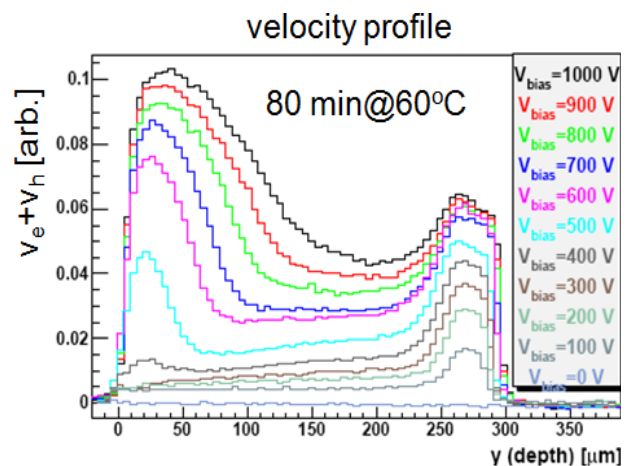
Figure 3: Velocity profile for the same detector as shown in Fig. 2.

- Long term annealing enhances the multiplication [2], due to two reasons. An increase of the concentration of effective acceptors leads to a higher peak in the electric field. The decrease of the effective trapping probabilities for electrons results in more electrons which are multiplied.

- Measured amplification profiles and multiplications factors are moderate (few times). The moderate increase of the amplification factor with voltage points to a moderation of the field by trapping of the holes and which reduces the negative space charge.

- The increase of the dark current correlates with the multiplied charge.

The effects of charge multiplication were also investigated in irradiated thin n-type epitaxial detectors in Hamburg [3]. The measured CCE for alpha particles showed a steep increase of the CCE at very high voltages for the most irradiated device. A CCE>1 was observed for the first time in pad detectors (see Fig. 4.). The measurements of the CCE with radiation of different penetration depths confirmed that most of the multiplication takes place in the high electric field close to the main junction. It is therefore essential to understand the impact of junction geometry on multiplication. Long-term measurements have also shown that the multiplication is stable in time and uniform within 1% over the pad detector surface. One difficulty is the high operating voltage required, which results in instabilities (micro-discharges) in both irradiated and non-irradiated detectors. This has been attributed to details of the sensor layout.

Epitaxial detectors of different thicknesses were also investigated with electrons from a ^{90}Sr-source. In terms of measured charge the thinner detectors performed equally or better at the same voltage (see Fig. 5), which is expected for the multiplication mode of operation. The beneficial effect of the multiplication for the signal can however also result in a significant excess noise. The signal-to-noise ratio was found to improve at high bias voltages due to the multiplication until the parallel (current) noise dominates the series (voltage) noise. The multiplication mode of operation is therefore

particularly suitable for segmented pixel detectors operated at low temperatures where the current noise per channel is small. The impact of the multiplication on the noise will be further investigated.

In order to understand the charge trapping and the multiplication mechanism in heavily irradiated detectors, a simulation program has been developed in Hamburg, which calculates for different deposited charges the pulse shape and the integrated current as function of the electric field, the charge trapping probability and the multiplication coefficient. The measurements can only be described, if a non-uniform space charge, and contrary to previous studies, a field dependent trapping is assumed. An effort to understand the electric field on the basis of microscopic defect levels which is under way in Hamburg will be discussed below.
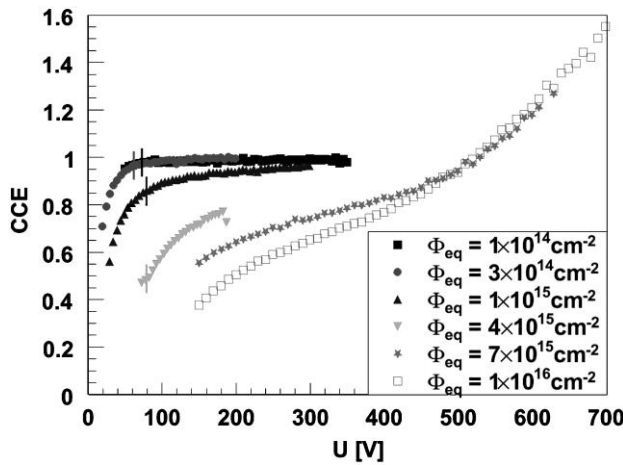

Figure 4: CCE in 75 μm thick n-type epitaxial pad detectors after different irradiation fluences of 23 GeV protons. The vertical lines indicate U_{dep} taken from capacitance–voltage (CV) measurements.
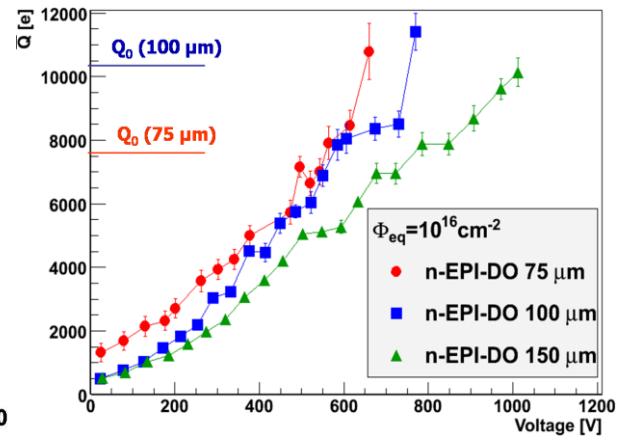
Figure 5: Collected mean charge as a function of bias voltage in epitaxial detectors of different thicknesses. Q_0 denotes the charge collected in the non-irradiated device of the given thickness.

Investigations of defects in epitaxial silicon detectors

The work of the Hamburg MC-student focuses on the study of radiation induced defects responsible for the degradation of silicon detector performance under irradiation and on the understanding of the electric field distribution. Several n-type materials, presently discussed as candidates for use at the SLHC, have been and are being investigated.

Comparative studies of the defects induced by irradiation in epi-DO (epitaxial silicon diffusion oxygen enriched) and epi-ST (Epitaxial standard silicon), orientation <100>, 100 μm and 150 μm thick, resistivity 300 Ωcm, irradiated with 23 GeV protons with fluences of 4×10^{11} cm^{-2} at the CERN Proton Synchrotron (PS) were performed. The change of the electrical properties of pad diodes was investigated by CV- (capacitance-voltage), IV- (current-voltage) and DLTS- (Deep Level Transient Spectroscopy; measurement of the temperature dependence of the capacitance transient due to the majority carrier emission of traps) measurements. It was observed that the radiation induced point defects (vacancy or interstitial coupled to an impurity) depend on the material, that defect engineering does work and that the cluster related defects are independent of the oxygen concentration. By annealing studies it was found, that the cluster related defects are responsible for the increase of the leakage current. To separate the contributions to the leakage current of the

different cluster defects, their concentrations for different annealing steps were determined and compared to the current. As seen in Fig. 6 a linear dependence of the density of two defects close to the middle of the band gap and the decrease of the leakage current was established. The direct correlation of cluster defects with the leakage current is a major step in the understanding of radiation damage in silicon
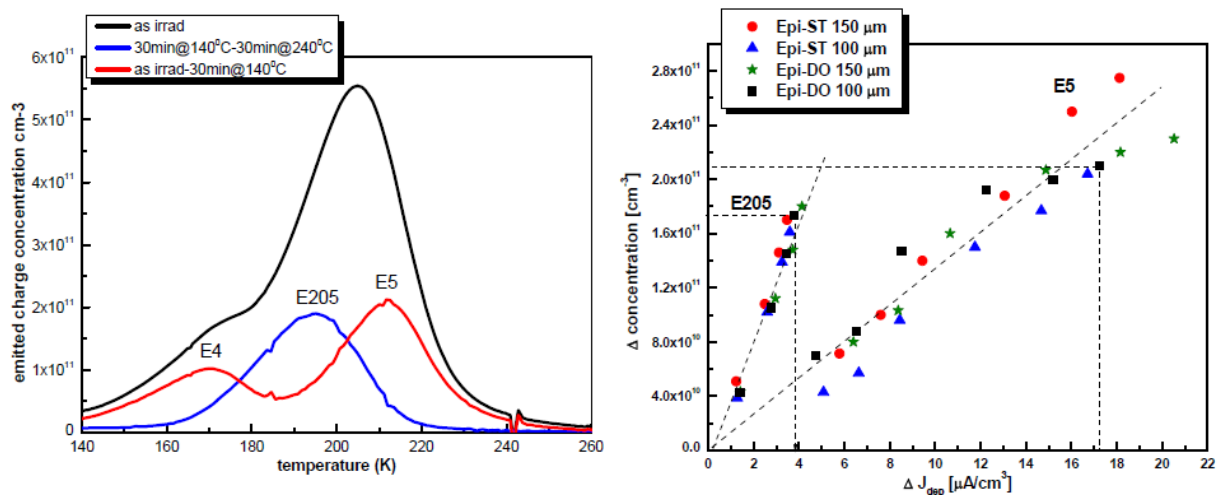

Figure 6: Results of the DLTS and current measurements for the epi-ST detector irradiated to 4×10^{11} 23 GeV protons/cm^2; left concentration of emitted charges; right correlation of the dark current density with the concentration of the two defects E5 and E205.

As discussed above, the detailed understanding of the distribution of the electric field in irradiated silicon sensors is still lacking. Therefore a complementary effort has been started using n-type STFZ (standard float-zone silicon), orientation <100>, 100 μm thick, resistivity 300 Ωcm, irradiated at the CERN PS with 23 GeV protons and at TRIGA (nuclear reactor) of the Jozef Stefan Institute (Ljubljana) with reactor neutrons with a wide range of fluences (10^{13} - 10^{15} cm^{-2}). Admittance Spectroscopy (measurement of the conductance and capacitance as a function of frequency at constant bias) and Thermally Stimulated Current Technique (TCT: recording of the current as function of temperature due to the thermal emission of carriers from deep states) are used. A change of the conductance and the capacitance as function of frequency is observed: At low frequencies the traps respond to the AC-signal, whereas at high frequencies the emission rate is too slow for this to happen. The frequency dependence of the capacitance and conductance is sensitive to the energies and the densities of the traps caused by the radiation. The depletion depth of the sensor is obtained from the capacitance extrapolated to low frequencies. Parallel to the measurements, a custom simulation program with a number of simplified assumptions is being developed. At a later stage detailed simulations using the commercial simulation program Synopsys-TCAD will be performed. First quantitative results and the demonstration of the validity of the method should be available by the end 2010.

[1] G. Kramberger et al., "Investigation of irradiated silicon detectors by Edge-TCT", IEEE Trans. Nucl. Sci. Vol. 57(4), 2010, p. 2294.

[2] G. Kramberger et al., "Annealing studies of irradiated p-type silicon sensors by Edge-TCT ", presented at Vertex 2010, to appear in Proceedings of Science.

[3] J. Lange et al., "Properties of a radiation-induced charge multiplication region in epitaxial silicon diodes", Nucl. Instr. and Meth. A622 (2010) p. 49.

[4] J. Lange et al., "Charge Multiplication Properties in Highly Irradiated Epitaxial Silicon Detectors", presented at Vertex 2010, to appear in Proceedings of Science.

Project 4: Micro Pattern Gas Detectors

High precision and ultra-low mass tracking detectors based on the GEM technology

Project Coordinator: Leszek Ropelewski, CERN

Marco Villa, ESR, CERN. Supervisor: Leszek Ropelewski

Jing Dong, ER, INFN LNF. Supervisor: Giovanni Bencivenni

Introduction

Micropattern Gas Detectors (MPGD), in particular GEM and Micromegas, provide many promising features relevant to the next generation of HEP experiments. These include: good position accuracy and two-track resolution, high counting rate capability, high radiation tolerance, time stability, as well as large flexibility of the geometrical shapes and readout schemes. Future experimental demands will push the requirements further, particularly in the areas of long-term performance at very high radiation fluxes, susceptibility to heavily ionizing background and to neutrons, increased geometrical dimensions and minimized materials budget.

CERN group is optimizing single mask GEM technology which allows building large area detectors. The R&D program consisted of the construction and evaluation of small size detector prototypes and the performance comparison with detectors of alternative technologies particularly Micromegas. New technologies are applied in the production of large size demonstrators for SLHC upgrade feasibility studies of TOTEM T1, CMS and ATLAS muon systems.

The **INFN LNF** group is working on an ultra-light, cylindrical and dead-zone free triple-GEM detector for the upgrade of KLOE detector, KLOE-2, at an upgraded DAFNE machine. The detector will be upgraded with the insertion of an Inner Tracker (IT) between the beam pipe and the Drift Chamber (DC) inner wall, composed by 4 concentric detection layers at radii from 15 cm to 25 cm from the beam line and with an active length of 70cm, based on the Cylindrical GEM detector (C-GEM) technology. The main requirements are: i) $\sigma_{r\phi}$ ~200μm and σ_z ~500μm spatial resolutions; ii) total material budget below 2% of radiation length, to minimize the multiple scattering effects before the DC volume. Each of the 4 layers of the IT will be a triple-GEM independent detector composed by: the cathode, the 3 GEM foils for the multiplication stage (gain ~10^4) and the anode read-out circuit. These electrodes are obtained from very light polyimide foils (100 μm thick for cathode, 50 μm for GEMs, 150 μm for anode) rolled-up to a cylindrical shape.

In this first period, the training project was concentrated on the following activities:

1. Optimization and evaluation of the single mask GEM technology.
2. Construction and test of the large area planar GEM detectors with single-mask GEM foils.
3. The study of the XV strip readout configuration at the H4-SPS beam CERN facility with a telescope composed by small, 100×100mm^2, planar GEMs in magnetic field with the first version of the dedicated GASTONE ASIC, a 64 channels chips specifically developed for the GEM detector.
4. Exploration of alternative Micromegas technology for HEP applications.

Single mask GEM technology optimization

GEMs are electron multiplication structures invented in 1997 by F. Sauli. The GEM base material is usually a 50 µm thick polyimide layer sandwiched between two 5 µm thick copper layers. In the standard manufacturing procedure, tiny holes of about 70 µm in diameter are created in the substrate by means of a photolithographic process, with the etching taking place from both sides of the substrate. Since both the raw material and the two masks are flexible, the alignment procedure becomes extremely involved when going to large area, limiting the maximum GEM dimensions to about 30 x 30 cm^2.

In single mask photolithography only one mask is used and the etching is performed layer by layer only one side. By using this new method one can produce GEMs with square meter area. The GEM holes have a conical shape and the holes diameter on both sides of the GEM electrode can be tuned as desired. The plot on Fig. 1 presents Monte Carlo GEM transparency study. It shows the fraction of electrons ending up on each electrode and insulator as a function of the holes geometry. x–axis presents the holes diameters [µm] on the top and bottom electrodes.

During development of the single mask GEMs the formation of a clearance around the holes in the top copper layer was observed. This clearance, known as *rim*, decreases the time stability of the gain due to charging up of the exposed plastic surfaces. In order not to create the rim, one has to protect the top electrode while etching the bottom one. This can be done by gold–plating the top electrode. However, the slightest delamination between copper and polyimide will lead to copper under etching and the creation of gold spikes which could favor discharges. Also electrochemical etching of the bottom electrode seems inappropriate. A possible solution is the use of electrochemical active corrosion protection. Here, a direct current flows from the top copper electrode to the walls of the etching bath, making the top copper inert to the action of the chemicals during the bottom copper etching. Fig. 2 is a cross–section of a GEM hole obtained in this way. The holes are perfectly defined, with no rim. The introduction of a very small rim can make these GEMs very robust, but the effective gas gain is quite small.
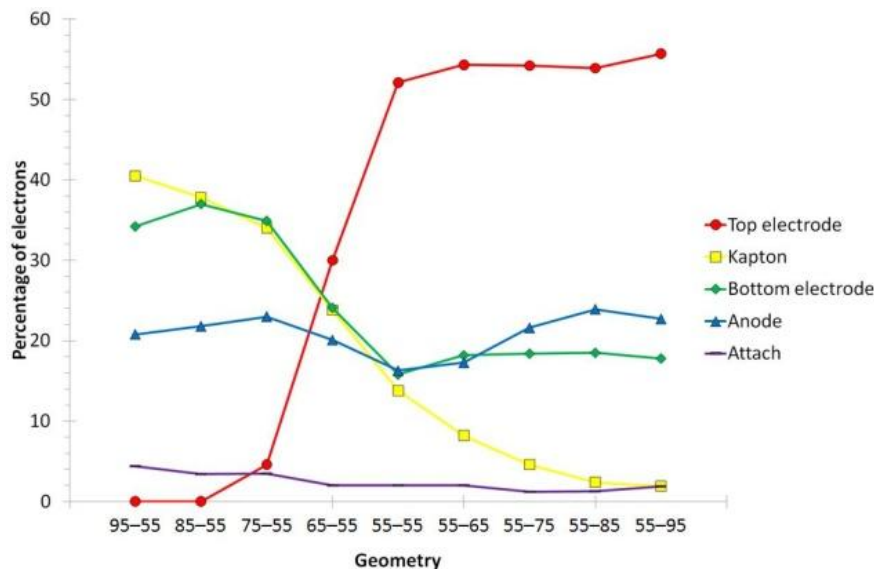

Fig. 2: Fraction of the electrons ending up on the different GEM electrodes as a function of holes geometry

A further refinement of the manufacturing process includes a polyimide post–etching. The holes in the polyimide have a biconical shape similar to standard GEMs (see picture on Fig. 3). These single mask GEMs have no rim, are robust and show a gain only a few percent lower than standard GEMs.

They can be used to cover large areas and they can be produced using roll–to–roll equipment. The price per unit area is expected to drop by two orders of magnitude with respect to standard GEMs in case of large volume production in industry.
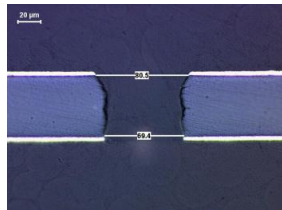

Fig. 3: Cross section of the GEM hole produced using active corrosion protection
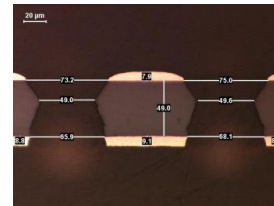

Fig. 4: Cross section of the GEM hole after polyimide post-etching

Large area GEM detectors

To build the KLOE-2 IT layer, a GEM foil as large as $1440\times700mm^2$ is needed. This foil can be made splicing three separate to $480\times700mm^2$ foils, produced using single mask technology.
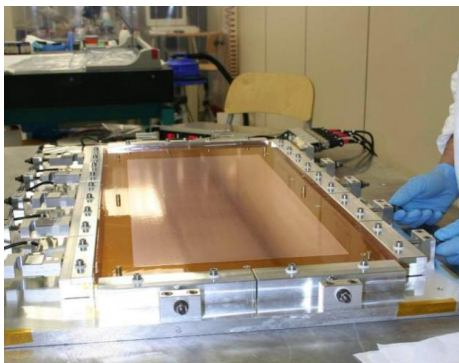

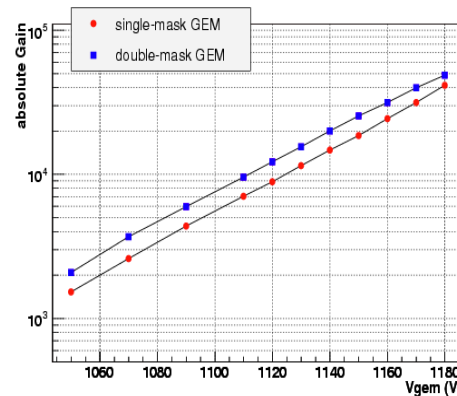**Fig. 5:** Tensioning tool for large area GEM foil.

Fig. 6: The effective gain for single and double-mask GEM as a function of the sum of the voltage applied on each GEM.

Performance comparison with standard, double mask GEM detectors is necessary due to the modified hole shape. In order to check the performance of the new single-mask GEMs over a large area, two large area planar GEMs ($300\times700mm^2$) were built. Dedicated tools for the stretching (Fig. 4), handling and assembling of such large foils have been designed and realized. The chambers, which are one of the largest GEM detectors ever operated, were equipped with the GASTONE 64-channel final release, readout with the Off-Gastone-Electronics (OGE) Board and flushed with Ar/CO_2 (70/30) and preliminary tested in current-mode with a ^{137}Cs source.

In Fig. 5 the gain for the different GEMs is shown. The gain of the single-mask GEM is about 25% lower than that of the double-mask. Fig. 6 shows the efficiency of the large chamber as a function of the sum of the voltage applied on each GEMs as measured with a 10 GeV pion beam at the T9-PS beam line.

Fig. 7 presents photo of a $990\times455 \ mm^2$ detector similar to one described above and constructed using single mask technology. Detector serves as a prototype for CMS muon system upgrade feasibility studies and has been recently tested in the RD51 beam facility in CERN SPS showing performance compatible with standard GEM detectors used in COMPASS, LHCb and TOTEM experiments. Data analysis is in progress. Similar smaller detector was constructed for T1 TOTEM upgrade project.
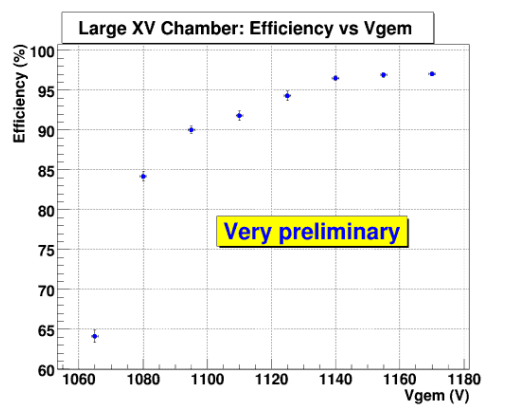
Fig. 7: The efficiency of the large XV chamber as a function of the sum of the voltage applied on each GEM.

Fig. 8: Large area triple GEM detector prototype for CMS muon system upgrade.

Small planar GEMs for readout studies for C-GEM readout

A typical orthogonal X-Y readout cannot be used for the KLOE-2 inner tracker due to its cylindrical geometry therefore a more suitable solution for the final design of the detector is a 2-D readout segmented with 650 µm pitch XV patterned strips. The X-V readout scheme is shown in Fig. 8.
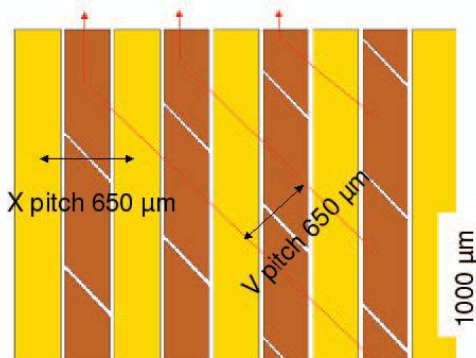

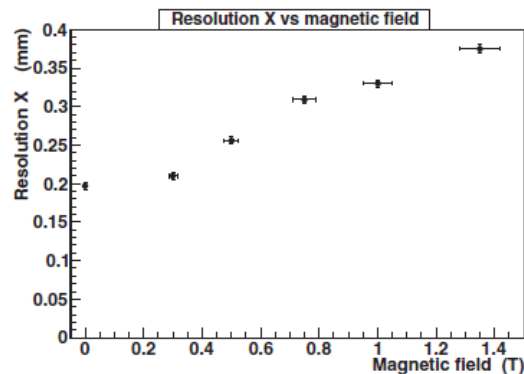**Fig. 9:** Scheme of the X-V readout configuration.

Fig. 10: Resolution on the X coordinate as a function of the magnetic field.

The investigation of possible problems correlated with this specific arrangement required a specific test. In addition, since the IT needs to operate inside KLOE's magnetic field, the effects on the readout and cluster of fired strips formation have to be studied. During KLOE data taking the magnetic field was set at 0.52 T. To improve the acceptance for low momentum tracks, the option with a lower magnetic field value, e.g. 0.3 T, is under study for the KLOE-2 project.

To address the issues of the XV readout and the operation in magnetic field, a dedicated test was done at SPS-H4 North Area RD51 beam facility at CERN. The H4 area is equipped with the GOLIATH magnet providing a field adjustable from 0 to 1.5 T perpendicular to the horizontal beam-plane (X-Z). For the test we used 150 GeV/c π^+ beam. The X-V readout was tested with a tracking telescope realized with five 100×100mm² planar triple-GEMs detectors with 650 µm pitch readout strip plane: four chambers were equipped with standard X-Y readout and the fifth with the X-V readout under investigation. The GEMs were partially equipped with 22 digital readout GASTONE boards with 32 channels each, four on each XY chamber and six on the XV chamber. The coincidence of 6 scintillators (30×30mm²) read-out by silicon photo-multipliers (SiPM) provided the trigger signal for

the acquisition. We have used the same working point as for the CGEM prototype: Ar/CO_2 (70/30) gas mixture and operating voltages V_{fields} = 1.5/2.5/2.5/4 kV/cm and V_{GEM} = 390/380/370 V (ΣV_G = 1140V).
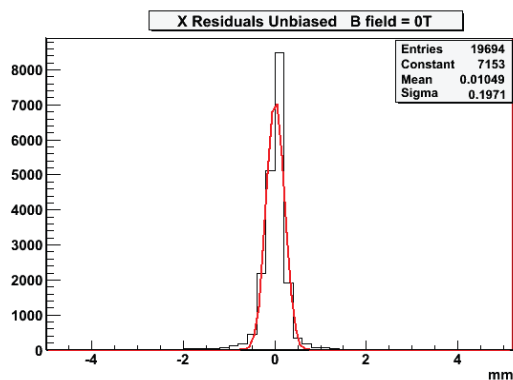

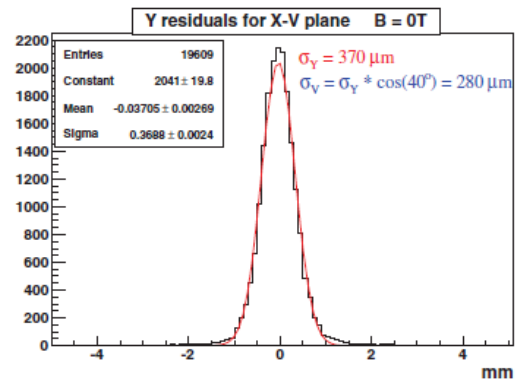**Fig. 11:** Residuals in the X view for the X-V readout GEM without magnetic field.

Fig. 12: Resolution on the V coordinate.

The XV chamber performance have been studied by measuring the spatial resolution defined as the sigma value from the Gaussian fit to the residual plot of the XV chamber. The spatial resolution obtained as a function of the magnetic field is shown in Fig. 9, while in Fig. 10 the plot of the residuals at B=0 T is reported. As one can see there is clear effect on the resolution with increased magnetic fields, due to the Lorentz force, which on our test-beam setup affects the X coordinate only (corresponding to the bending plane). The resolution on the X coordinate ranges from 200 μm at B=0 T up to 380 μm at B=1.35 T. The resolution on the V coordinate is ~280 μm corresponding to ~370 μm on the Y coordinate, Fig. 11.

As shown in Fig. 12 the increase of the magnetic field, leading to a larger spread of the charge over the readout strips, causes a reduction of the charge seen by each single pre-amplifier channel, with a consequent efficiency drop. As a consequence the increase of the magnetic field requires for higher gains in order to efficiently operate the chamber.
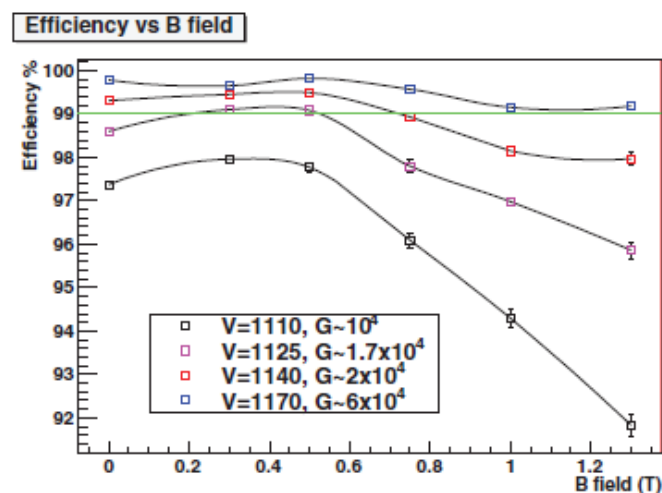

Fig. 13: Resolution on the X coordinate as a function of the magnetic field for different detector gains.

Micromegas performance optimization for muon detection

Micromegas detectors were invented in 1996 by Y. Giomataris. Micromegas are two-stage parallel plate detectors: the primary electrons created in the drift gap migrate towards the anode, where an

auxiliary electrode is used to create a high field region. The bulk technology is a recent development which exploits photolithographic techniques to create the amplification gap. A woven metallic grid is encapsulated between two layers of photoimageable film and, after the development of the film, only little pillars remain to keep the grid in place

The MAMMA collaboration is exploring the possibility of using large area bulk Micromegas for upgrading the forward region of the ATLAS muon system. The possibility of reducing the spark rate by means of a GEM preamplification stage was studied. The combined detector was tested with x–rays and 6.4 MeV alphas. The results are summarized in the plot on Fig. 13. The x–axis shows the total gas gain, while the y–axis represents the spark rate normalized with the number of alpha particles. The black points are obtained with a Micromegas only, the red points with a GEM preamplification at fixed voltage and the green points in the ideal situation in which both the Micromegas and the GEM voltages are scanned. One can conclude that the GEM can reduce the spark rate by one order of magnitude.
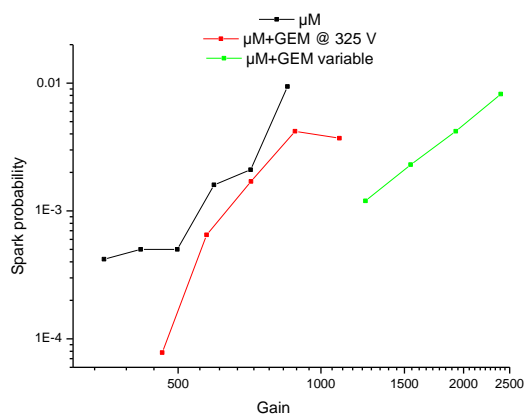

Fig. 14: Discharge probability as function of the gas gain in different GEM + Micromegas detector configurations
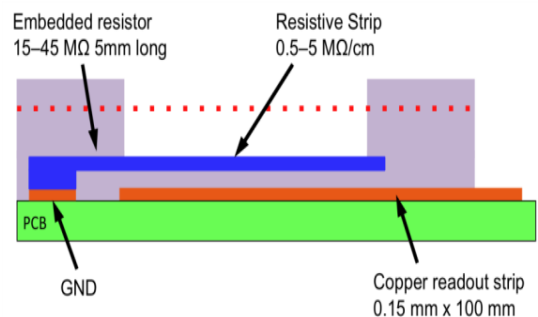

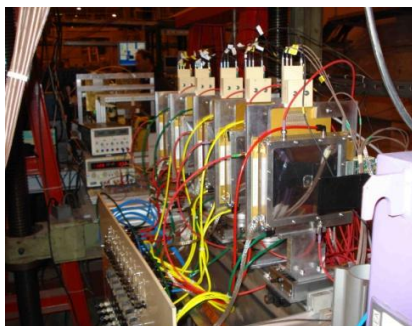**Fig. 15:** Cross section of bulk Micromegas detector with capacitive coupled resistive strips

Fig. 16: Experimental setup of several resistive bulk Micromegas detectors in the MAMMA beam facility.

Fig. 17: Large size bulk Micromegas prototype for ATLAS muon system upgrade.

A recent achievement is the realization of bulk Micromegas with capacitive coupled resistive strips. Fig.14 shows a cross–section of such detector. The copper readout strips on the PCB are covered with an insulator and then with a resistive strip which is grounded through a resistor of some tens of MΩ. Detectors with different strip resistivity and with different ground resistor were tested with x–rays, in pion (Fig. 15) and in a neutron beam facilities, comparing the results with a standard bulk Micromegas. Data analysis is in progress. The resistive detectors show no mesh voltage drop and much lower current spikes. Moreover, the new technology can be scaled up to large areas (Fig. 16), thus making resistive Micromegas a good candidate for the ATLAS muon system upgrade for SLHC.

Conclusions

1. Single mask GEM technology was successfully optimized allowing construction of several large area prototypes meeting SLHC upgrade requirements and with performance compatible with standard GEM detectors used in COMPAS, LHCb and TOTEM experiments.
2. Two planar KLOE-2 prototypes with 300×700mm^2 foils have been built which showed in current mode good stability, uniformity, efficiency and a gain around 25% lower than double-mask GEM. KLOE-2 and the Cylindrical-GEM project are approaching steadily the finalization.
3. The KLOE-2 R&D program including XV readout characterized in magnetic field has been accomplished.
4. R&D focused on alternative Micromegas technology is well in progress; discharge probability, major drawback of this technology, is significantly reduced, what opens perspective for applications of large area, cheap and robust detectors in the field of muon detection.

Project 5: TPC with MPGD Readout

Project Coordinator: Ties Behnke, DESY Hamburg.

Rahul Arora, ESR, GSI. Supervisor: Christian Schmidt.

Stefano Caiazza, ESR, DESY. Supervisor: Ties Behnke.

Rolf Schön, ESR, NIKHEF. Supervisor: Els Koffeman.

1 Introduction

Time projection chambers (TPC) are used in many experiments in physics at accelerators. Within this project two main applications are studied: a TPC for a central tracker at a future linear collider, and a TPC at experiments at the GSI FAIR facility.

Time projection chambers offer many advantages if used as tracking detectors. They provide a large number of well measured points in three dimensions, can be built to a low material budget, and can be used to instrument large volumes efficiently. The readout of TPC's with micro pattern gas detectors is an attractive option to improve the resolution, to reduce the ion backdrift, and provide an overall very robust system.

The focus of the work in this workpackage is on the application of micro pattern gas detectors to readout the time projection chambers. In two projects GEM foils are used to instrument a large volume TPC. In a third group a novel option, the integration of the gas amplification device and a pixelated readout system into one detector, is studied.

2 Development of a GEM based TPC for a detector at the International Linear Collider

Work carried out by ESR Stefano Caiazza, DESY

The tracker at the proposed experiment for a future linear collider relies on a large scale high performance TPC. The requirements on resolution and efficiency are very challenging, and significantly exceed those achieved at existing systems. To achieve these performance goals the ILD TPC cannot use the traditional gas amplification systems, i.e. multi wires chambers, but must rely on micro pattern gas detectors (MPGDs). These devices have amplification structures which are of order of the anticipated resolution, around 100μm. This technology is relatively new, being developed in the last decade and has never been used in a TPC of the size foreseen for the ILD detector. To test these technologies and to validate and choose the best solution for the ILD detector a large prototype (LP) of the ILD TPC has been built by the LC-TPC collaboration.

One of the main features of this prototype is the possibility to accommodate seven independent and exchangeable readout modules in its anode endplate. With this tool several technologies were

already tested. The goal of the project is to develop a new module to be used in this large prototype, using GEMs as gas amplification devices.

The design of the module was constrained by the allotted size of the LP modules. We also decided we wanted to build a system which could achieve a point resolution better than 100µm for the entire drift length of the LP, with the maximum sensitive area and minimizing the dead spaces. Finally we decided to follow-up on a new technology developed at DESY in the previous years to build the GEM stack that is using a ceramic support structure instead of the traditional plastic frames.

The module design effort was split in four work packages:

Assembly backframe: This aluminium frame provides the mechanical mounting for the module in the LP endplate. It is also used to fix and align the other elements of the module.

Pad readout board: This element is the sensitive part of the detector. To achieve the required resolution we choose a pad size of 1.12×5.85 mm^2, for a total of about 5000 pads. Because no analogue electronics with a small enough footprint exists that can be mounted directly on-board, all the signals are routed to external electronic units. Moreover this board must deliver the high voltage for the GEM to operate, which complicates the design further.

GEM foils: The GEM foils for the module are produced at CERN, with a hole size of 50µm and a pitch of 140µm. They have been custom designed to fit the space allotted for the module and, to avoid destructive discharges due to the amount of electrostatic energy stored in the device, one of the two electrodes has been sectioned in four independently powered areas. The GEMs have been designed to allow for a stack of up to four elements to be built (3 amplification foils and a gate).

Ceramic Grids: The most innovative element of this design is the self-supporting ceramic structure which supports the GEMs, and defines the space between the GEM foils. These elements are laser cut in the same shape as the GEM, with an internal grid that supports the GEM from the inside limiting its sagging without requiring complicated stretching procedures during the assembly and reducing the amount of dead space introduced by the supporting structures. One of this grids, aligned with one of the GEMs can be seen in Figure.

Figure 1: The GEM foil and its ceramic support structure aligned before the gluing.

The whole module assembly is shown in **Figure wh**ere one can see the backframe to which the pad readout board and the GEM stack are mounted. The GEM stack itself is composed of several ceramic grids sandwiching a GEM foil.
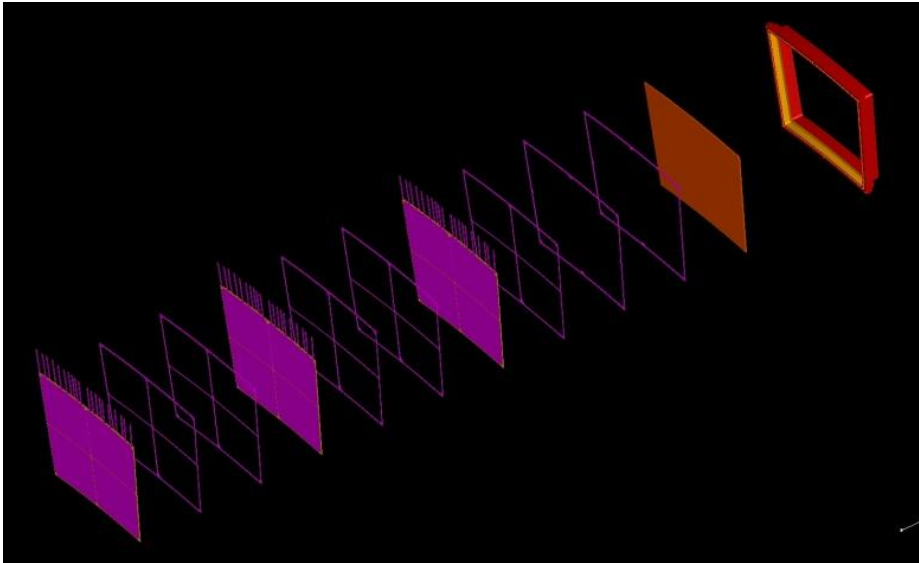

Figure 2: Exploded view of the DESY GEM module.

To commission the module before using it in the large prototype, we designed and built a commissioning system, composed of a drift chamber able to house a single module and multiple DAQ systems to perform different tests on the module. The drift chamber has a variable drift length up to 10 cm and hosts a system that house one or more radioactive sources to illuminate the module. In the near future the first module will be commissioned in this box, and tested under high voltage and with a radioactive source.

The next step then is to install the first module in the large prototype, and to operate it with beam. Following this first test, we will try to optimize the system to achieve the required resolution and to build more modules to be finally able to equip the whole endplate with seven modules and test them both in electron and hadron beams

3 Study of discharges in MPGDs

Work carried out by ESR Rolf Schön, NIKHEF.

A novel way to read-out micro pattern gas detectors is by integrating the detector and the readout chip into one structure. GridPix is a micro pattern gas detector (MPGD) consisting of a Micromegas-like amplification grid on top of a pixelated read-out chip (Timepix) with a size of 14 mm × 14 mm, studied at NIKHEF in the detector development group. When ionizing radiation hits the detector, the atoms in the gas volume are ionised and the resulting electrons are drifted towards the grid by an electric field between grid and a cathode while the ions drift to the cathode. An amplification field between grid and anode chip is used to accelerate the electrons further to the anode and to multiply them by creating avalanches. The charge is then large enough to be detected by the chip where further signal processing (pre-amplification and shaping) takes place (see Figure).
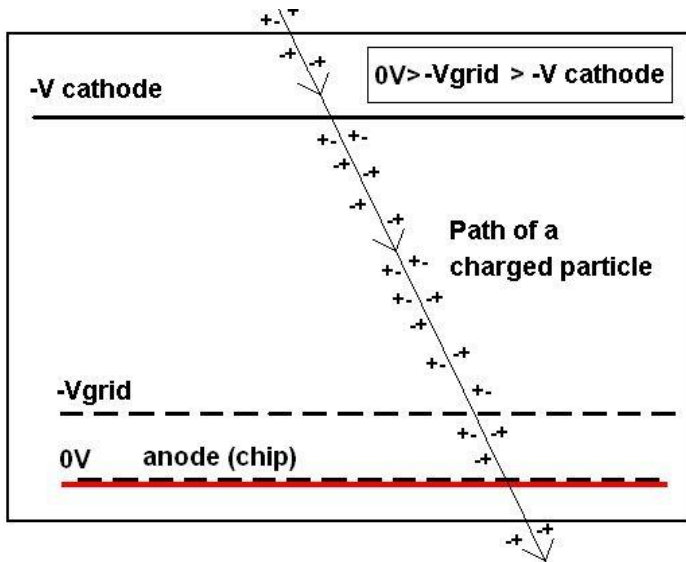
Figure 3: Principle of operation of the GridPix detector.

During the amplification process the electron avalanche can grow to a long plasma filament (a so-called streamer) able to connect cathode and anode and therefore producing a discharge. Consequently a lot of charge is deposited at the chip surface that, in extreme cases, can melt parts of the grid and/or the chip surface. But since the pixels are interconnected such an incident does not lead to the malfunction of only one or a few pixels but to the destruction of the whole chip and thus the detector.

To prevent the detector being destroyed by a violent discharge (also known as spark) a thin layer of resistive material has been used to cover the chip. Materials that have proven good performance for this purpose are hydrogenated amorphous silicon and Si-enriched silicon nitride (SiRN) (see Fig. The discharge can now be drawn away by the whole surface of the chip. As a result, sparks still appear but are not harmful to the detector anymore.
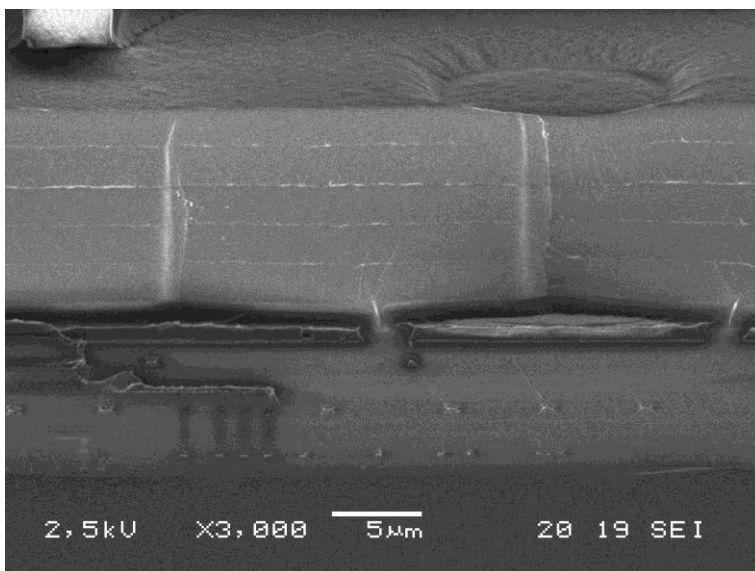

Figure 4: SEM picture of SiRN layer.

Of course, charging up of the resistive layer becomes important at high event rates. The purpose of this study is to investigate further the properties of this resistive layer, and to optimise its properties. The work in this area has just started, so that no results can be reported. Recently a set of data were systematically reported at CERN for two gas mixtures which will be used to study the behaviour of the GridPix detector in the near future.

4 TPC with MPGD Readout

Work carried out by ESR Rahul Arora, GSI.

The Project P5 at GSI is about the prototype studies of a TPC (Time Projection Chamber) detector with GEM (Gas Electron Multiplier) as amplification stage. The main objectives of this project are the central tracking upgrade of the FOPI experiment at GSI and the central tracking candidate for the PANDA experiment in the future facility FAIR (Facility for Antiproton and Ion research) at GSI.

A Time Projection Chamber detector is the perfect choice for the inner tracking detector device because of its low material budget and the very good resolution for hits and tracks. The gas detector also offers capability to identify particle types via dE/dx, the specific energy loss. The design of the prototype detector is shown in Figure.
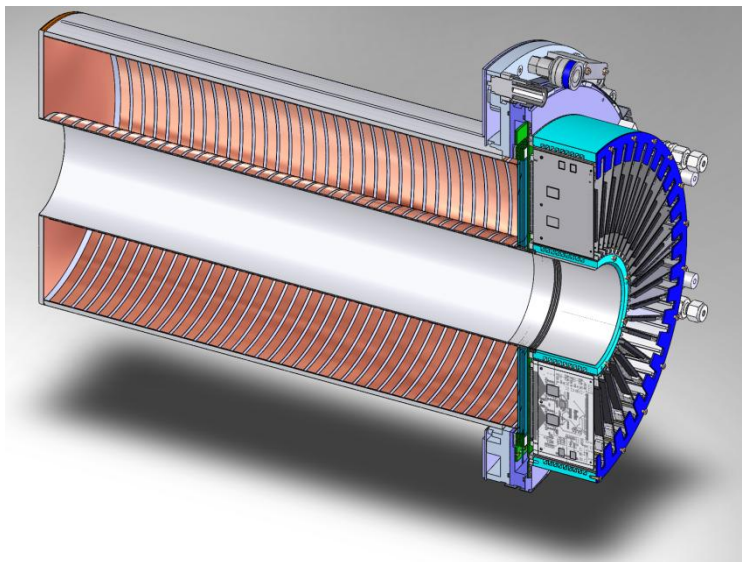

Figure 5: Picture of the TPC assembly

The Drift Length of the prototype detector is 725 mm. Stacks of three GEMs are used for the amplification. The inner diameter of the chamber is 105 mm and the outer one is 300 mm. Triple GEM stacks are used as amplification stage. The gain is of the order of several thousand with gas mixture of Ar-CO2 (90:10).

A GEM consists of an insulating foil, typically Kapton, clad on both sides with a thin layer of copper. Holes are present in the foil and the copper connecting both sides. If a potential difference is applied to the two copper surfaces, a strong electric field develops in the holes. For 400 V across a single GEM, produces the field of about 50kV/mm which causes the avalanche multiplication of the electrons with gas.

At first, leakage current measurements for the GEMs were performed. The GEMs were tested for leakage current at about 600V at a relative humidity of 1%. The currents were found to be in the expected ranges of a few nA. Some of the foils with higher currents had to be discarded.

After the satisfactory tests the GEMs are glued on frames and then assembled in the GEM Flange. After assembling the GEM Flange with Media Flange and a pad plane we get the GEM detector without the field cage. There were tests done on the detector for gas tightness, material stability in high voltage and out gassing. The results so far are promising and as expected. The detector was first tested without the field cage to check gain uniformity of the GEMs as well as the total gain of the detector. The first tests were promising with a gas mixture of Ar-CO2 (70:30) at a scaling factor of up to 1.07 of the nominal voltages. The source employed for the tests was Fe55 with 5.9 keV X-ray K-alpha line. The no. of primary electrons produced was about 210 for this gas mixture. The gain of the detector was about 5100 for scale factor of 1.02 and 10000 for 1.07. After the complete assembly of the detector with Field Cage, cooling for FE cards and other accessory sensors, the detector was commissioned in the FOPI experiment in the first week of Nov. 2010 and data could being taken.

At first, data were taken with cosmic rays, later with beam. Some screenshots during data acquisition are shown in Figure. Depicted are the first tracks caused by cosmic rays in the experimental area where a trigger was supplied by two scintillating paddles above and below the chamber. The tracks in the picture above are taken with a 1.4GeV Kr beam on an aluminium foil as target. There are 30000 Kr ions per spill. Each spill lasts for 10 sec, generating almost 500 triggers per spill. The drift field for these measurements is 260 V/cm in Ar-CO2 mixture (90:10).
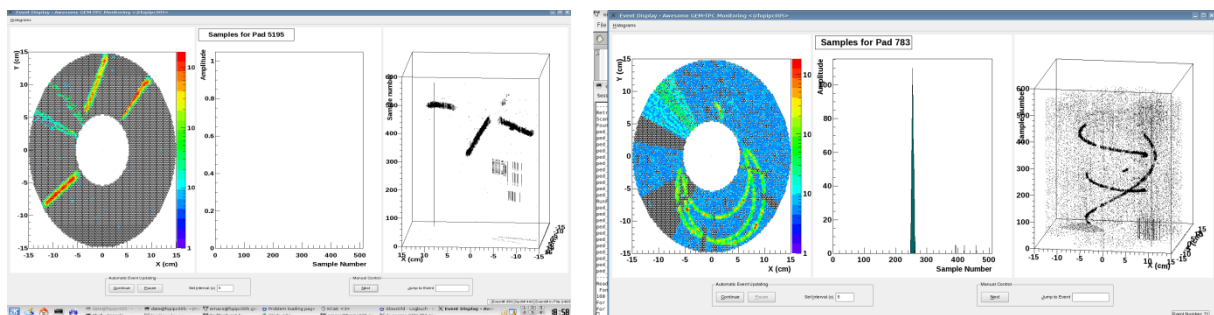
Figure 6: Pictures of first tracks recorded with the prototype chamber in beam.

The gas flow through the TPC was about 90 ltr/hr with an oxygen content of 66 ppm. The chamber was operated in an axial magnetic field of 340 mT.

In summary the target set in the project for the initial year has been achieved within the time period assigned. The next task is to do the analysis of the data from the detector for the detector performance as well as physics issues. The detector design revision is also done in the coming time period.

Project 6: Very Forward Calorimetry

Project Coordinator: Wolfgang Lohmann, DESY Zeuthen.

Olga Novgorodova ESR, DESY. Supervisor: Wolfgang Lohmann

Jonathan Aguilar, ESR, AGH Cracow. Supervisor: Marek Idzik

At future electron-positron collider detectors special calorimeters are needed in the very forward region. In the current detector concepts two calorimeters are foreseen - BeamCal for luminosity optimization, and LumiCal for the precise luminosity measurement.

The technologies to build these detectors are developed within an international collaboration, FCAL. The research work of the ESRs is embedded in the FCAL activities.

Using GEANT4 simulation tools (MOKKA, BeCaS, Lucas) the performance of the calorimeters is compared for different designs. In addition, more realistic simulation tools have been developed. These ongoing studies have already led to results important for both the technical design and the physics benchmarks of the detector. One such important effect in LumiCal is due to non-instrumented regions in the sensor plane - the 2.5 mm-wide gaps between sensor tiles placed azimuthally around LumiCal. These gaps cause a signal loss (leakage) and deteriorate the energy measurement, as shown in Figure 1.
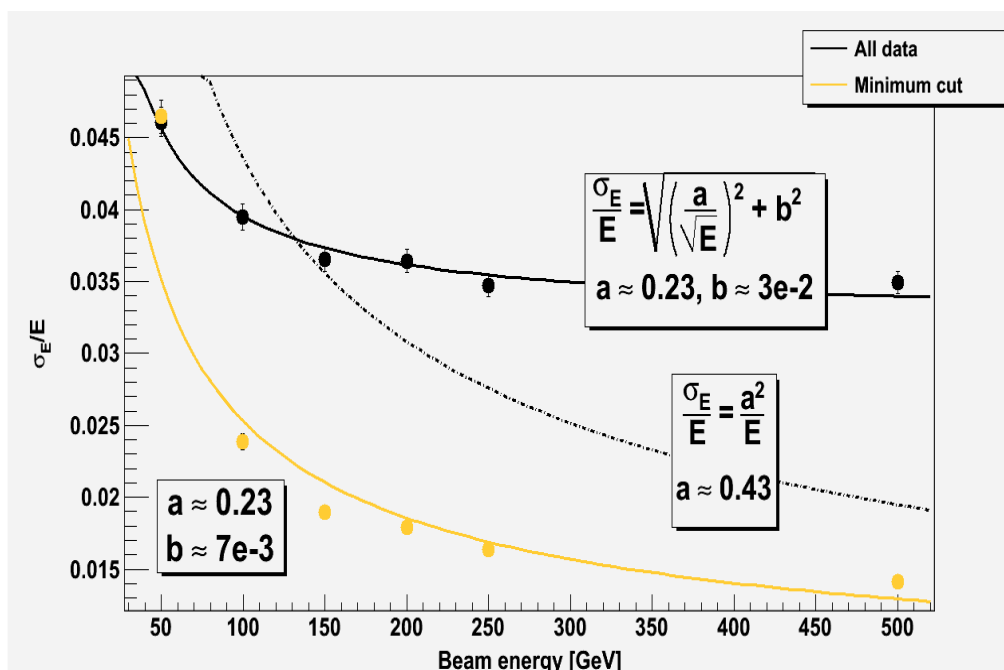

Figure 1: Energy resolution in LumiCal for different models - no leakage term (black, dotted line), all particles (black, solid line), and gap particles excluded (yellow line).

Both ESRs participated in a test of the radiation hardness of solid-state sensors performed at the ELBE accelerator at Dresden-Rossendorf.

Recently major effort has been invested in the assembly of sensors with front-end electronics. Segmented BeamCal and LumiCal sensor prototypes have been designed, produced and measured in the laboratory. In parallel, front-end ASICs have been developed and tested in the laboratory. The measured parameters of both components matched the criteria defined by the physics performance requirements. As a major step towards a full system test, sensors of both types have been assembled with front-end ASICs to form a sensor plane prototype. For this purpose fan-outs made of

flexible printed circuit boards are used to connect the pads to the ASICs using wire bonds. The first tests in the laboratory gave very promising results, so we decided to test the system in a particle beam.

For readout of the system the data acquisition system from the CMS beam conditions monitor has been adopted.

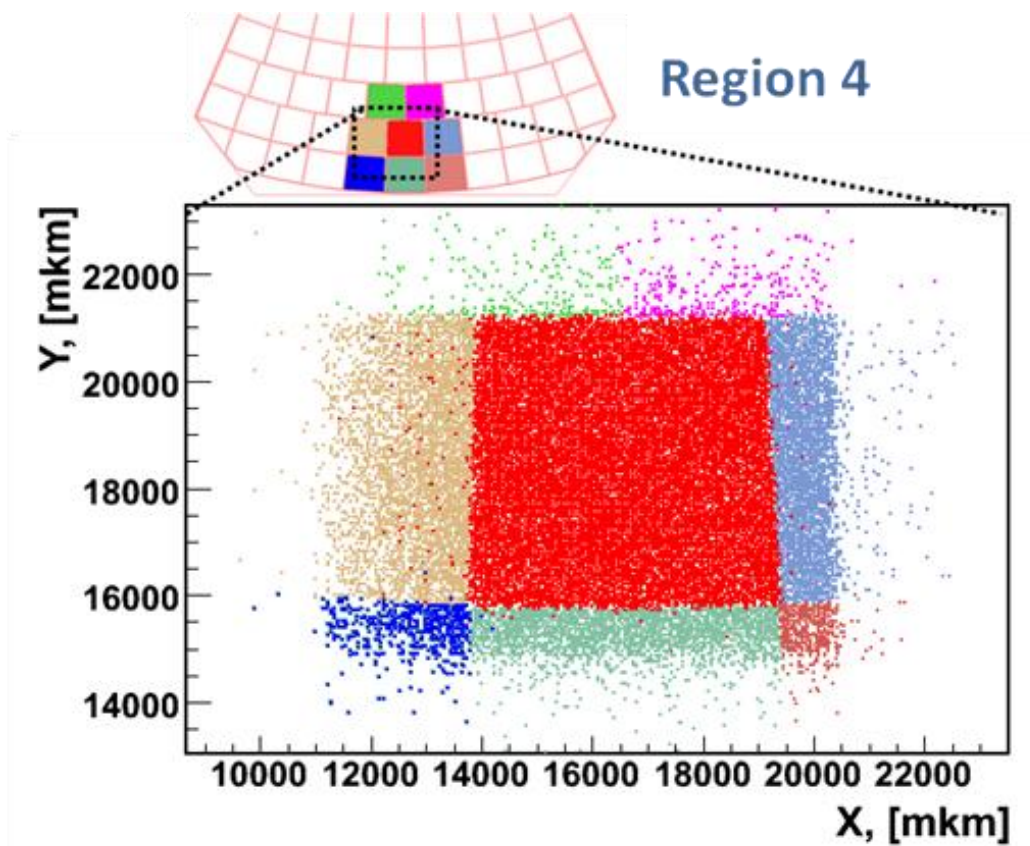Figure 2: Reconstruction of the impact point in the detector box

Fully assembled sensor plane prototypes were installed inside of a silicon strip detector telescope (MVD) from ZEUS. The whole setup was positioned in the 4 GeV electron beam at DESY.

The MVD measures the track of beam particles to high precision and therefore enables the point of impact on the sensor plane under test to be calculated.

On both sensors, several regions were covered by the beam and a few million triggers were recorded, both in the central region of the sensors and at the edges.

After alignment and reconstruction of the tracks the impact point on the sensor can be compared with the signal on the pads. An example (using preliminary results) is shown in Figure 2. The pattern of the pads is clearly visible.

The analysis of the test-beam data is still ongoing. Preliminary results on the charge collection efficiency (CCE), signal to noise ratio (S/N), crosstalk and uniformity of CCE near the pad edges are very promising and have been presented at conferences and collaboration meetings.

The test-beam venture was supported by other FCAL members and summer students and partly supported by EUDET.

The analysis of the test-beam data will be finished within the next months. In parallel, the ESRs are involved in preparation of the forthcoming beam tests and completing the readout system, consisting of an ADC ASIC connected to the FE ASIC.

Olga Novgorodova also participated in data acquisition and analysis at the fast beam conditions monitor BCM1F at the CMS experiment, to acquire experience in the operation of similar sensors in a running experiment and to investigate possible application of the sensor plane prototype at LHC.

Both ESRs have attended all MC-PAD training events and reported about the results of their research work on meetings of the FCAL collaboration and at international linear collider workshops. The results also become part of several publications and conference proceedings.

Olga Novgorodova is a Ph. D. student at the Brandenburg University of Technology in Cottbus, Germany. Jonathan Aguilar is a Master's student at the AGH University of Science and Technology in Cracow, Poland.

References:

- "Forward Instrumentation for ILC Detectors", arXiv:1009.2433, accepted by JINST.
- "Studies on the Electron Reconstruction Efficiency for the Beam Calorimeter" arXiv:1006.3402, Proccedings of the International Linear Collider Workshop, Beijing 2010.

Project 7: Advanced Photodetectors

Project Coordinator: Christian Joram

Paolo Beltrame, ER, CERN. Supervisor: Christian Joram

1. The Axial PET

1.1   Introduction

Excellent spatial resolution and high sensitivity are crucial aspects for Positron Emission Tomography (*PET*) imaging devices. In addition, the combination with Magnetic Resonance Imaging (*MRI*) is becoming essential. The Axial-PET (*Ax-PET*) project aims to prove the capability of a new PET instrument. This apparatus will be capable to produce biological images free from parallax error, and to improve independently the sensitivity and the resolution – without the need to stoop to compromises, as it happens in the standard PET. As additional feature Ax-PET can also provide the possibility to discriminate Inter Crystal Scattering (*ICS*) events and operate in the presence of magnetic field, therefore together with MRI.

1.2 The working principle

The basic principle of this novel detector consists in an axial arrangement of long scintillation *LYSO* crystals around the Field Of View (*FOV*) and Wave Length Shifter (*WLS*) strips orthogonally positioned to the crystal direction.
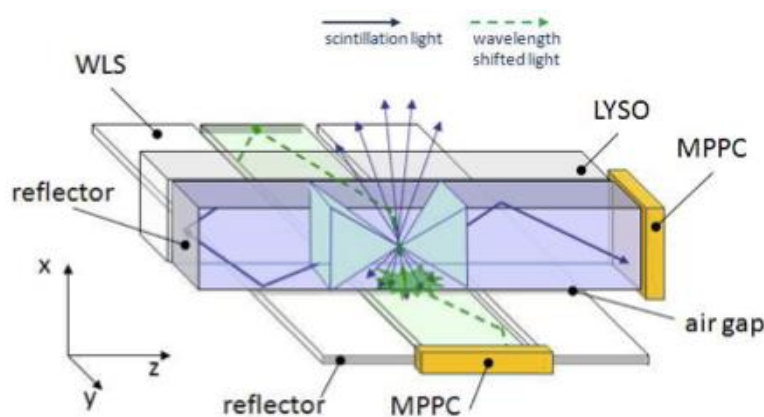

Fig 1. Simplified drawing (with two LYSO crystals and three WLS strips) describing the main principle of the Ax-PET. The scintillation light derived from the interaction of the impinging photon (coming from the top) is trapped inside the crystal and, by means of internal reflection, reaches the photon detector (MPPC) on one side, whilst on the other is reflected by aluminum reflector. The escaping light from the LYSO is collected by arrays of WLS strips, and subsequently read out in order to localize the axial position of the photon interaction inside the crystal.

The crystals – placed on different layers one behind the other – provide information on the *x* and *y* (*transverse*) position of the 511 keV gamma ray point of impact, and on the energy release by the

photon interaction. The WLS strips – fixed in layer of arrays just back each crystal layer and collecting the light escaping from the crystal sideways – allow a precise determination of the *z* (*axial*) coordinate by means of a center of gravity clustering technique.

A simplified scheme (showing two crystals and three strips) of the working principle is sketched in Fig. 1.

1.3 The project

The aim of the collaboration has been the construction of a two modules demonstrator. Each module consists of 48 LYSO crystals (St. Gobain), 10 cm long with a cross section of 3×3 mm^2, assembled in a stack of 6×8 bars, and 26 WLS strips of 0.9×3×40 mm^3, placed on top of each crystal layer. The optical photons in the LYSO are read out by Multi Pixel Photon Counters (MPPCs) from Hamamatsu (S10362-33-050C, 3600 cells (50×50) ⌈m^2, dimension (3×3) mm^2 active area). The MPPCs for the WLS readout are custom designed (OCTAGON-SMD, 782 cells (70×70) ⌈m^2, dimension (3.22×1.19) mm^2). The signals are amplified and fed into a 128 channel self-triggering readout ASIC VATAGP5 (Gamma Medica-IDEAS), controlled by a VME DAQ system.
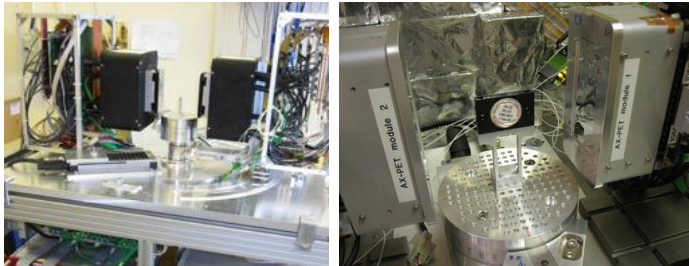

Fig 2. Left: Picture of the two module demonstrator. It the image is possible to see the radioactive source mounted in the middle on a rotating gantry and the second module on the rotating harm. Right: zoom on the two modules and on the point-like source.

To mimic the performances of a full ring camera, the two modules have been mounted face-to-face, on a table with a rotating gantry holding the radioactive source in the middle. Therefore, by rotating the source, it has been possible to reconstruct the image from different perspective angles. Moreover, to extrapolate the performances with an extended field of view, the second module of the demonstrator has been mounted on a horizontal rotating harm allowing to displace the modules out of the 180° alignment. The whole demonstrator can be seen in Fig. 2.

1.4 Point-like source measurements and results

First measurements with [22]Na point-like radioactive sources have demonstrated the validity of the detector design principle and of the set-up. In Fig. 3 left the typical energy spectrum of a single LYSO bar exposed to 511 keV photons from the [22]Na source is shown. In Fig. 3 right the energy resolution, selecting event with different crystal multiplicity, is shown.
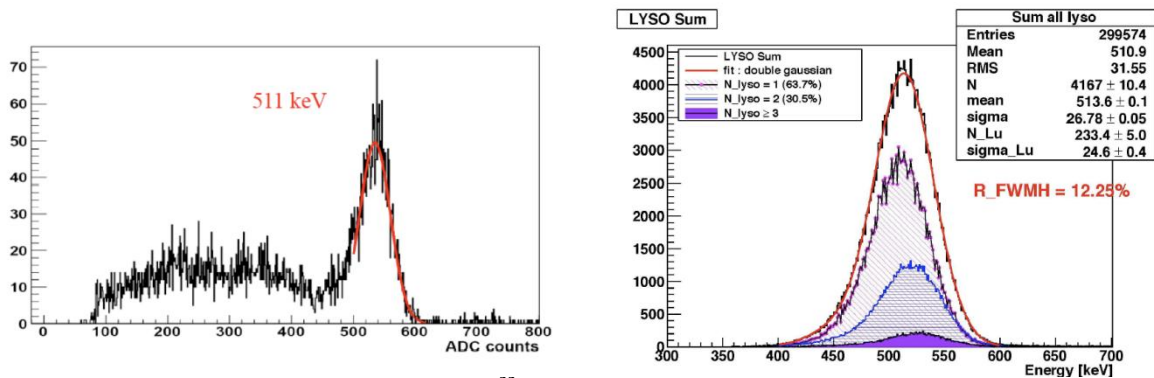
Fig. 3. Left: Energy spectrum obtained using a ^{22}Na point source. Right: Summed energy spectra of the LYSO crystals at different crystal multiplicities (NLY SO = 1, 2, 3 or more).

As for the spatial resolution, in the transaxial plane (x, y) the resolution is limited by the size of the crystals i.e. 3×3 mm^2 cross-section yielding $\sigma_{x;y}$ = 0.87 mm. In the axial direction the final resolution achieved is σ_z = 0.64 mm, once the contribution coming from the positron range and the source finite size is subtracted. In Fig. 4 the image reconstruction of the point-like source using the geometrical intersection of the Line Of Response (LOR) is shown.
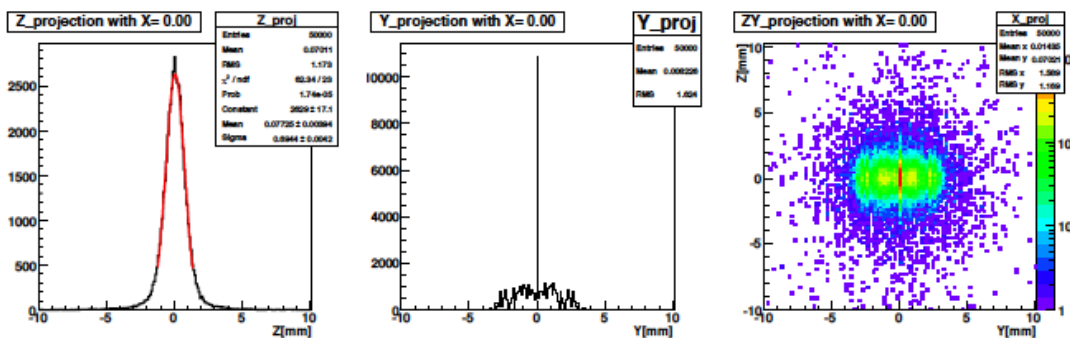

Fig. 4. Simple bidimensional geometrical reconstruction of the position of the source achieved with the intersection of all the detected LOR. The transaxial (x, y) coordinate is assigned as the center of the hit LYSO crystal (discrete value), the axial z coordinate is derived from the center of gravity method on the WLS cluster (continuous value).

Dedicated Monte Carlo code for the detector simulation has been developed and an excellent agreement with data has been found.

1.5 Extended source measurements and status of the project

The demonstrator performances have been further tested in measurement campaigns, in collaboration with the ETH-Zurich and the AAA company at Saint Genis, using extended sources – capillaries or phantoms. Fig. 5 shows a picture of the micro Derenzo phantom with the corresponded reconstructed image.

Thanks to the very promising results achieved, the project has been presented in several conferences and described in several publications.[1] An overall paper describing the feature and the

---

[1] P. Beltrame, *Demonstration of an Axial PET concept for brain and small animal imaging*, proceedings in publication on Nuclear Instruments and Methods in Physics Research Section A http://dx.doi.org/10.1016/j.nima.2010.07.017 (2010).

performances of the demonstrator is in preparation and will be soon submitted to *Nuclear Instruments and Methods*.
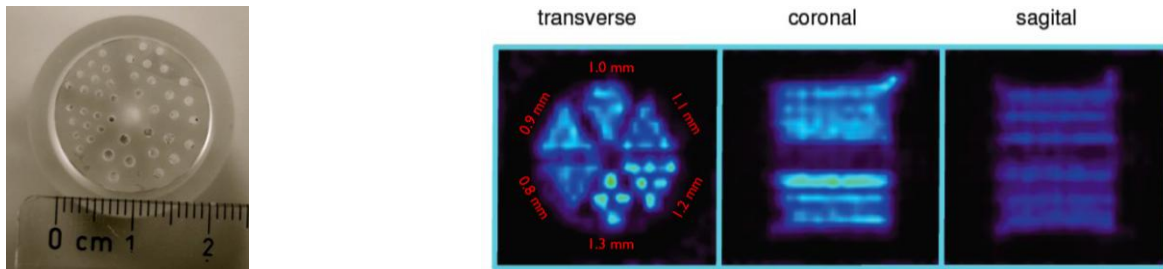

Fig. 5. Right: Micro Derenzo phantom. Right: preliminary reconstructed image of the phantom.

The collaboration has also recently started cooperating with Finnish institutes and companies to study possible commercialization.

2. The ATLAS-ALFA detector

2.1   Introduction

An accurate knowledge of the *LHC* luminosity is crucial for a precise determination of both Standard Model processes and New Physics discoveries, and for precision measurements involving the Higgs boson. The *ALFA* (Absolute Luminosity For ATLAS) detector consists in a high-precision scintillating fiber tracker designed to determine the absolute LHC luminosity at the ATLAS interaction point (*IP1*) with a precision at the level of ~3%.

2.2 The detector

The ALFA detector is mounted on the so-called Roman Pots (*RP*), which permit to approach the LHC beam axis to about 1.5 mm distance. The whole detector is made of eight RPs placed 240 m faraway from the IP1, four at each side, going in pair from the top and from the bottom. A drawing of the ALFA detector installed down into the LHC tunnel is visible in Fig. 6, together with a zoom of one RP and a more detailed view of the detector.
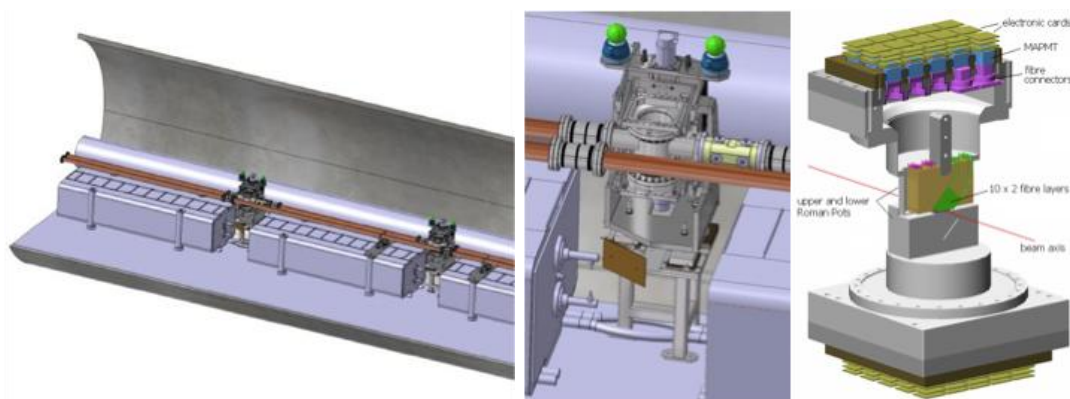

Fig. 6. Left: Detector installation inside the LHC tunnel. Center: zoom of a Roman Pot station. Right: detailed view of the main detector components.

The aim of the experiment is the tracking of the elastically scattered protons at very small polar angles – at the level of 3.5 μrad.

Each ALFA station has a Main Detector (*MD*) consisting of ten layers. Each layer is made by two plates arranged at +45° and -45° respectively, and each plate has 64 scintillating fibers of 0.5 mm^2. The fibers are coupled to 64 channels Multi-Anodes PhotoMultipliers Tubes (*MAPMT*).

Each detector has two so-called Overlap Detectors (*OD*), whose purpose is to provide information on the relative vertical positioning of the two main detectors. The ODs consist of three layers of two times 30 scintillating fibers horizontally aligned.

2.3 The test beam measurements

The detectors have been subject of different test beam campaigns in 2009 and in 2010. The last campaign has involved all the 8 ALFA detectors and for the first time also the ODs have been put in operation together with the whole ALFA devices. In Fig. 7 right, a photo of the test beam area with the ALFA detector is shown. Fig. 7 Left, shows the occupancy plot of the beam profile. The two MDs are visible as the two diamond shapes, in red and in blue, for the upper and the lower detector, respectively. The four rectangles visible at the side represent the ODs.

2.4 Status of the project and feasibility studies for a possible upgrade

The measurement campaigns have shown that the detector performances are compatible with the requirement needed to perform a precise determination of the absolute luminosity. The data collected in 2009, fully analyzed, have demonstrated a spatial (vertical and horizontal) resolution of the main tracker detector of the order of 50 μm and a uniform trigger and detection efficiency close to 100%.

The analysis of the 2010 data is on the way. One of the goal will be to show the capability of the OD to determine the relative positioning of the main tracker with an accuracy better than 10 μm. The installation of the whole RPs into the LHC tunnel is foreseen to be completed for the beginning of 2011.

In parallel, a feasibility study for the upgrade of the ALFA MD is in progress. The aim of this project is the replacement of the MAPMT readout by means of MPPCs. For this purpose four S10984-100P MPPC (1×4 channels, each channel having 100 cells of 100×100 μm^2 size), plus one as spare, from Hamamatsu have been purchased. Preliminary tests will be performed using a left-over plate of the ALFA main detector, connecting four fibers to each MPPC to build a 16 fibers tracking detector.
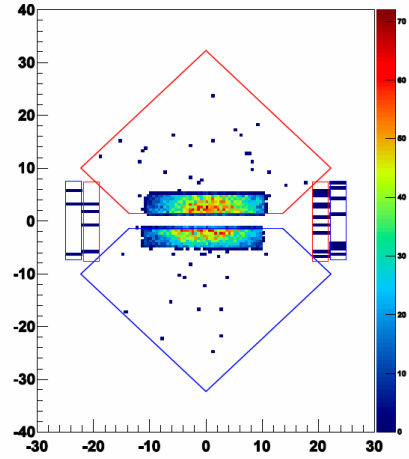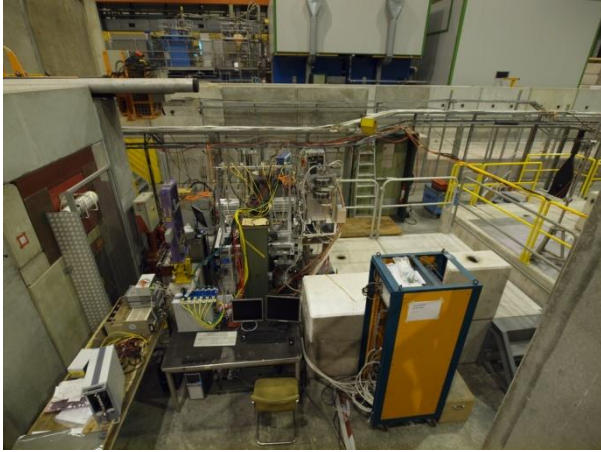
Fig. 7. Left: Detector installed inside the test beam area at CERN. Right: Beam profile as shown by the analysis software. Dimensions of the different part of the detector are not in scale.

Project 8: Photodetectors for High-B Fields

Project Coordinator: Samo Korpar, JSI Ljubljana.

*Ruben Verheyden, ESR, JSI Ljubljana. Supervisor: Sami Korpar.*

Photo-detectors for particle identification in high energy particle physics experiments and for scintillation detectors for multimodal medical imaging often have to operate in magnetic fields exceeding 1 T. In addition, they are required to efficiently detect single photons. While the traditionally used photomultiplier tubes (PMTs) do not work in high magnetic fields, standard semiconductor light sensors (photo-diodes, avalanche photo-diodes (APDs)) are not sensitive to single photons. The aim of this project is to develop photo-detectors compatible with high magnetic fields and investigate their application for particle identification and medical imaging. The sensors under study are Geiger mode APDs (also known as silicon photomultipliers, SiPM) and micro-channel plate (MCP) PMTs with multi-anode read-out. There are two main activities within the project: one concentrates on characterization of SiPMs and aims to construct the PET module suitable for use in a time-of-flight PET, and the other aims to construct the ring imaging Cherenkov (RICH) detector prototype with aerogel radiator and MCP-PMTs for detection of Cherenkov photons.

The use of SiPMs as photon detectors in PET modules offers several advantages over conventional light sensors, including application in a magnetic field, more compact design and easier operation. SiPMs from different manufactures are being assessed in a characterization set-up, and in a PET apparatus consisting of LYSO scintillation crystals coupled to a silicon photomultiplier array.

Single SiPMs are being tested in a characterization set-up consisting of a pulsed picosecond laser (PiLas, 34 ps FWHM) to determine device properties including gain, geometrical efficiency, response linearity and timing resolution. Extensive tests have been performed with SiPM prototypes from STMicroelectronics with an active area size of 3.5x3.5 mm² and 4900 micro cells. The SiPM characterization set-up was placed in a temperature controlled environment allowing characterization in the range of -20°C to 20°C. From the measurements we have determined the surface sensitivity at room temperature, and have investigated the dynamic range and gain as a function of temperature. The surface scans showed that active area follows the internal structure of the SiPM which can be seen by the microscope, and the obtained geometrical efficiency agrees with the area covered with APDs.

A single SiPM PET detector was assembled by coupling a LYSO crystal from Saint-Gobain (Prelude 420™, 3x3x30 mm^3) to a STMicroelectonics SiPM to determine its feasibility for use as a time-of-flight PET (TOF-PET) photo-detector module. Energy and back-to-back timing resolution of this PET system were measured using the annihilation γ rays from a ^{22}Na source. Energy resolution of the PET system has been shown to be correlated to the over-voltage (the difference between bias and breakdown voltage) applied to the SiPM and is in the range of 12.5% - 17% (FWHM). Back-to-back timing resolution was measured to be in the range of 330 ps - 400 ps (RMS). Obtaining an optimal timing resolution requires to work at single photo-electron signal heights. High dark noise rates of SiPM devices at the single photo-electron level (several 100 kHz/mm^2 of active SiPM area at room

temperature) make it beneficial to lower the temperature of the device. At a temperature of -20°C it was possible to obtain a back-to-back timing resolution of ~330 ps (RMS).
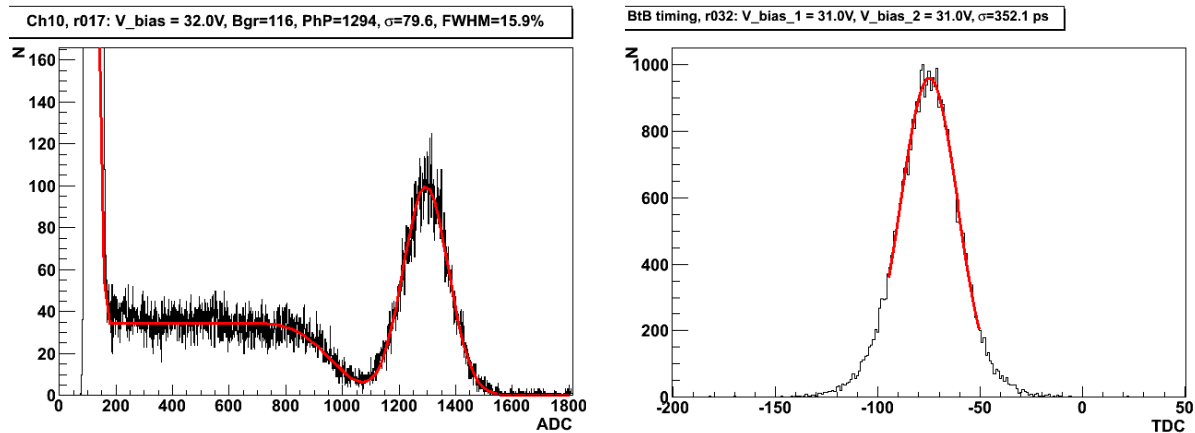
Examples of energy spectrum (left) and back to back timing distribution (right, 25 ps/TDC channel) measured with single SiPM modules.

For the next step of the project, two pairs of PET modules have been constructed by optically coupling SiPMs to a 4x4 array of LYSO crystals (4.2x4.2x20 mm^3 at 4.5 mm pitch, Saint-Gobain and Sinocera). One module uses an array of 4x4 SIPMs from Photonique (PCB-PET-07, 2.4x2.4 mm^2, 1700 micro cells), and the other Hamamatsu MPPCs (S10931-100P, 3x3 mm^2, 900 micro cells). The modules will be tested in a small scale PET demonstrator. This will enable the comparison of energy, spatial and timing resolution of the SiPM array modules with a module using multi-anode PMT's.
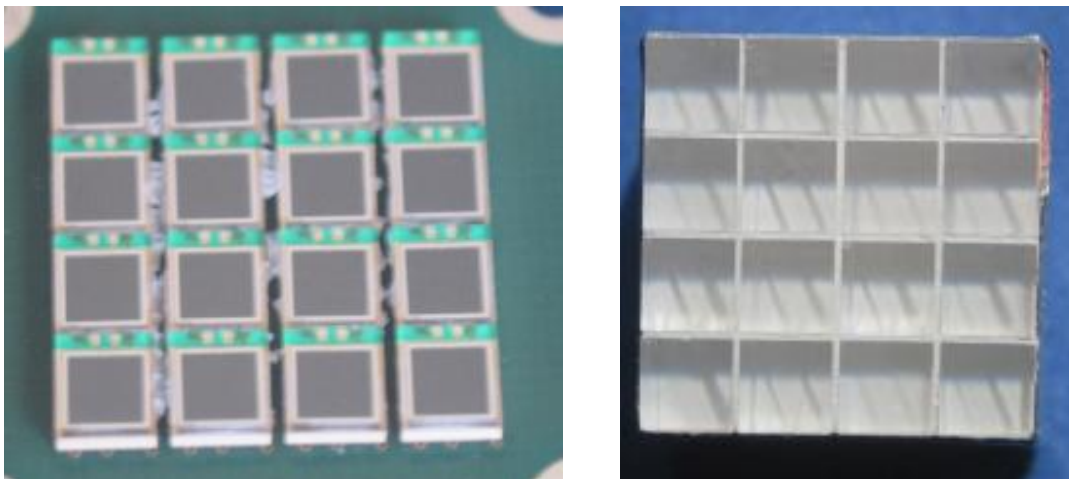
Array of 16 (4x4) Hamamatsu MPPCs (left) and matching array of LYSO crystals (right).

Due to a very large dark count rate of SiPMs, a novel type of read-out electronics may be needed to improve the time resolution (in particular in TOF-PET applications and in the detection of single photons in RICH counters). A waveform sampling read-out chip (BLAB) was investigated for this purpose.

The proximity focusing RICH counter prototype utilizes a Cherenkov radiator consisting of two layers of silica aerogel with different refractive indices, the higher being downstream. Such an arrangement results in a focusing effect of the Cherenkov rings originating in each layer and

41

improves the angular resolution. An array of multi-anode MCP-PMTs is used as photo-detector and is placed after a short expansion gap of 20 cm from the radiator entrance surface.

A multi-anode MCP PMT with 10 μm diameter pores developed by Photonis was investigated as a detector of single photons. The sensor was shown to perform well in high magnetic field up to 1.5 T. To evaluate its long-term stability in particle physics experiments, its performance was studied as a function of the charge, accumulated on the anode. During the test MCP-PMT was illuminated with blue LED so that single photon rate on each channel was around 1MHz. About 10% decrease of quantum efficiency was observed after total accumulated charge of 400 mC/cm^2.

Preliminary tests of RICH prototype were done in November 2009 using a 2 GeV/c electron test beam at KEK in Tsukuba (Japan). The RICH counter consisted of an aerogel radiator and two Photonis multi-anode MCP-PMTs covering about 30% of the ring. Multi-wire proportional chambers were placed in front and behind the RICH counter to provide particle tracking information. The measured Cherenkov angle resolution and the number of detected photons show that a pion/kaon separation of 4σ is possible at particle momentum of 4 GeV/c.

A new prototype of a RICH counter is being finalized which contains six MCP-PMTs and will be tested by cosmic rays and in the beam.
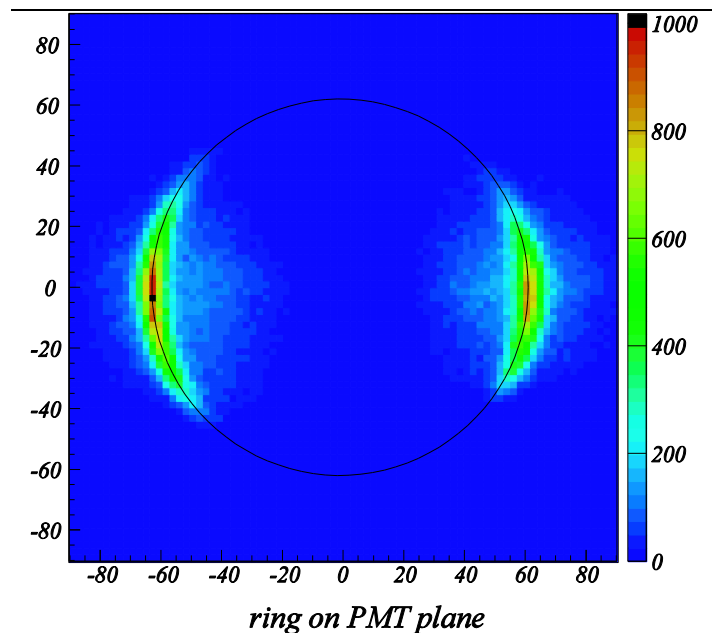
Photonis multi-anode MCP-PMT (left) and parts of the Cherenkov ring detected during the 2009 beam test (right).

Project 9: Front-end Electronics for Hybrid Pixel Detectors

Project Coordinator: Els Koffeman, NIKHEF

Francesco Zappon, ESR, NIKHEF. Supervisor: Els Koffeman

Introduction

GOSSIPO-3 is a prototype chip developed in 130nm IBM technology in a joint effort between Nikhef (Netherlands) and the Bonn University (Germany) to be used for the read-out of Micro Pattern Gas Detectors (MPGD). The chip has been designed to test several circuits such as two different Low Drop Out (LDO) voltage regulator to bias the fast oscillator and a high resolution Time-to-Digital-Converter (TDC) together with other components (charge sensitive amplifiers, discriminators, control logic). In every chip there are two pixels: one with the complete analog front-end and the TDC and the other with only the digital block, the latter allows us to test and characterize the pixel without any analog interference. The digital block contains a state machine that controls three counters which can operate in two different modes: in timing mode both the Time over Threshold (ToT) and the Time of Arrival (ToA) are simultaneously recorded while in hit counting mode the counters are reconfigured to record the number of hits arriving in a programmable time window. The three counters are named Fast (4 bit, 1.7 ns resolution), ToT (8 bit, 6.4 µs dynamic range) and Slow (12 bit, 102.5 µs dynamic range).
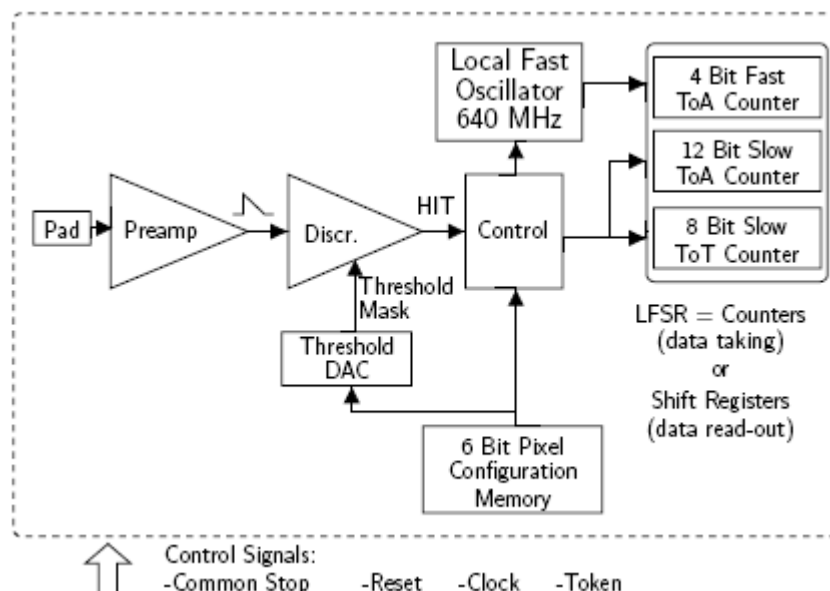

Fig. 1: Pixel block diagram

The design phase of the chip took place at the end of 2008/beginning of 2009 and the chip came back from the factory in March 2010.

Working principle:

When a particle traverses the detector its charge is collected and shaped by the front-end electronics: if the signal is above threshold, the discriminator "fires" to signal the start of the acquisition. At this moment, the fast oscillator is started and it is stopped by the first rising edge of the system clock (40 MHz); the number of fast clock cycles is recorded in the Fast counter. At this point the ToT and the Slow counter start to count: the former stops when the signal goes below the threshold, while the latter stops when the Trigger signal (common stop) arrives. After the data taking phase, the Token is sent to the chip to start the serial read-out of the pixel content: the counters are reconfigured as one big shift register clocked with the 40 MHz system clock. If the Token is not sent, the internal state machine automatically reset and it becomes ready for the next acquisition.
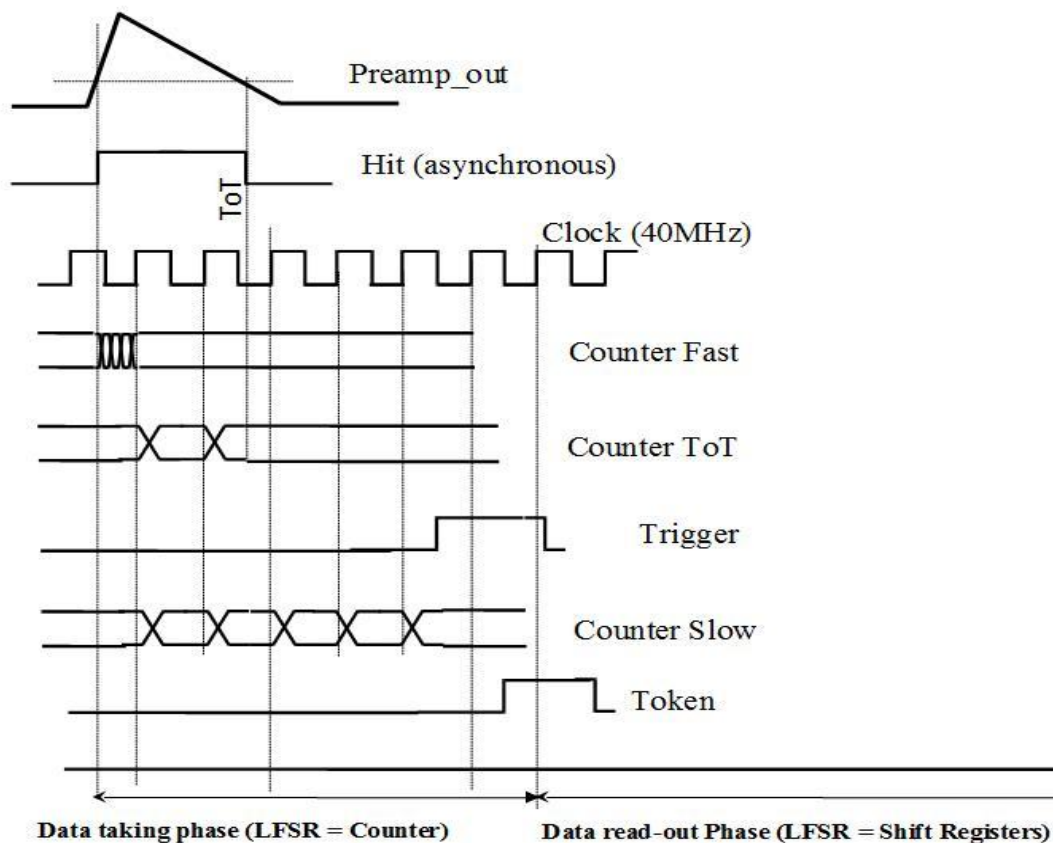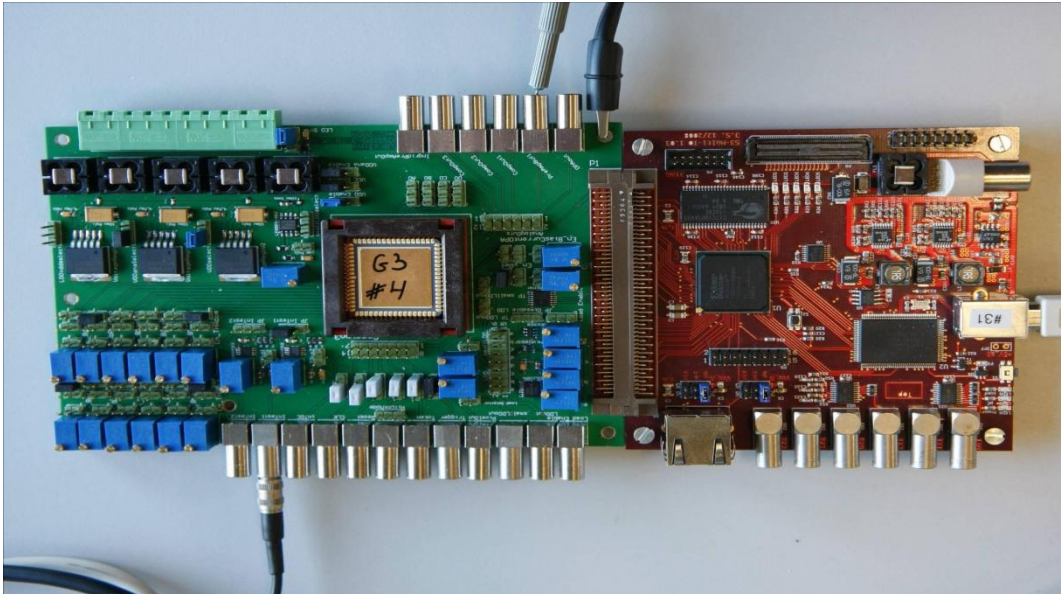
Fig. 2: GOSSIPO-3 timing diagram

Fig. 3: Test setup: on the left the G3 board, on the right the S3-MultiIO board with the FPGA

Data Acquisition

The Data Acquisition program has been developed using the well known S3 MultiIO FPGA board built in Bonn. This board houses a digital IO port with 100 pins, LEMO connectors, a clock generator and a Xilinx Spartan-3 FPGA fully programmable via USB (driver provided both for Windows and Linux) or JTAG. A complete set of custom functions written for the board make the code writing process straightforward. The DAQ interface has been developed in C++ (Microsoft Visual Studio 2010) using the Qt libraries 4.7.0 for the GUI while the FPGA control code has been written in Verilog using the Xilinx ISE environment 12.1.

Data analysis

A complete characterization of the TDC and the readout was the main goal of the tests conducted at Nikhef. In particular, one important aspect is the reproducibility and stability of the TDC's bin-size: ideally, we expect a bin size of 1.7 ns given by the oscillation frequency of the fast oscillator that is present in every pixel. To test this characteristic a delay scan has been performed: the hit signal, provided by an external pulse generator (Agilent 81110A) controlled using the DAQ interface via GPIB, is delayed with step of 0.1 ns: in this way, every 1.7 ns, we can see the transition from one count to another of the fast counter and every 25 ns from one count to another of the slow counter.

To fully characterize the transition region a fit with an error function has been performed: the fit parameters are:

- the 50% point of the curve, that is used to define the bin width

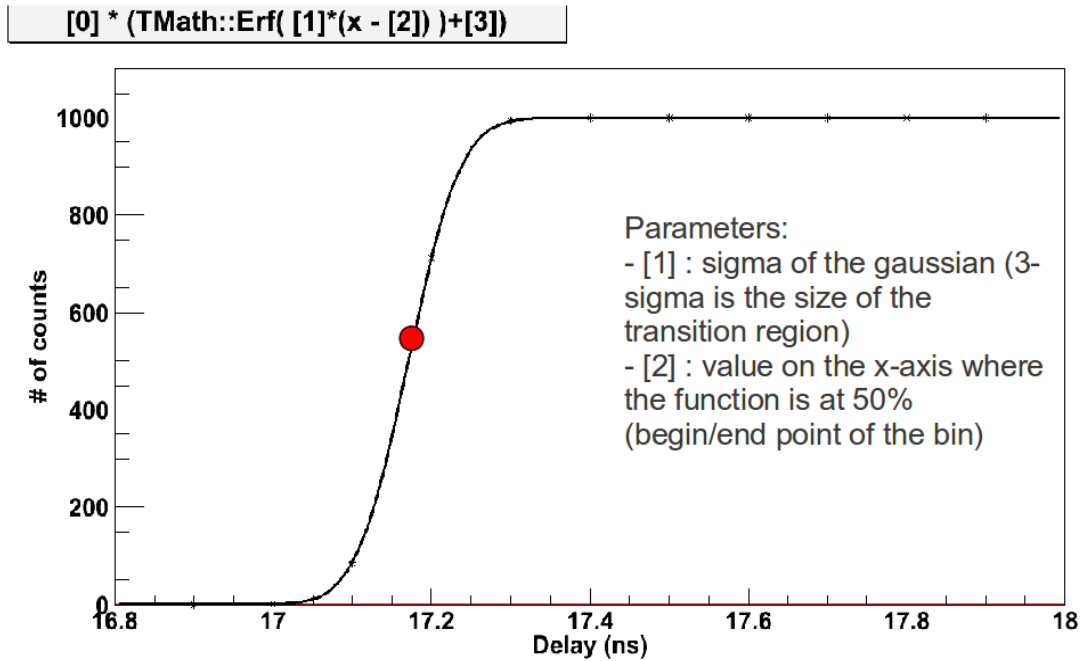- the jitter (σ of the Gaussian)

Fig. 3: example of a fit performed in the transition region

These two parameters allow us to characterize the TDC calculating the bin width, the time jitter, the Differential Non Linearity and the Integral Non Linearity. The results obtained until now can be found in the table.

Chip	Bin size (ns)	Error	Jitter (ns)	Error	DNL (%)
1	1.7525	0.3217	0.052	0.006	19.90
2	1.7524	0.1834	0.046	0.006	19.80
3	1.7520	0.1662	0.046	0.004	18.40
4	1.7567	0.2331	0.045	0.003	14.70
6	1.7548	0.2117	0.045	0.005	15.30
8	1.7551	0.1958	0.050	0.007	24.18
9	1.7540	0.2933	0.064	0.009	23.90
10	1.7550	0.2891	0.048	0.004	39.28

Conclusion

From the results obtained we can conclude that the chip is working as expected. The bin width is reproducible and the variation from chip to chip is not significant. Still, there are some characteristic to understand: in fact, bin number 7 and 8 of the fast counter show a difference in width wrt to the others bin. This is probably caused by crosstalk with the Clock signal since it is possible to observe this behavior in all the chip; moreover, bin 0 is supposed to be smaller (half of the normal size) by design, but what we see is that the bin is a bit smaller than expected and this could be explained

again with the crosstalk. To investigate this phenomena a study with a 20 MHz clock will be performed: this will avoid any transition of the Clock in the bin 7 and 8 position, thus the bin width should be the one we expect. In addition, the complete characterization of the analog front-end will be performed together with a threshold scan study.

Project 10: Monolithic Detectors

Project Coordinator: Henryk Palka, IFJ-PAN

Mohammed Imran Ahmed, ESR, IFJ-PAN and AGH-US, Supervisors Henryk Palka and Marek Idzik.

Tests of a monolithic CMOS SOI pixel detector prototype INTPIX3

Silicon pixel detectors are used in HEP experiments for precision measurements of charged particles trajectories, offering intrinsic resolutions of few μm, which is difficult to achieve in any other position sensitive detector. Pixel detectors that are used now are of a hybrid type: a detector and readout electronics are realized in separate silicon wafers interconnected with bump bonding. They are thick detectors which preclude their use in experiments where multiple scattering effects must be minimized.
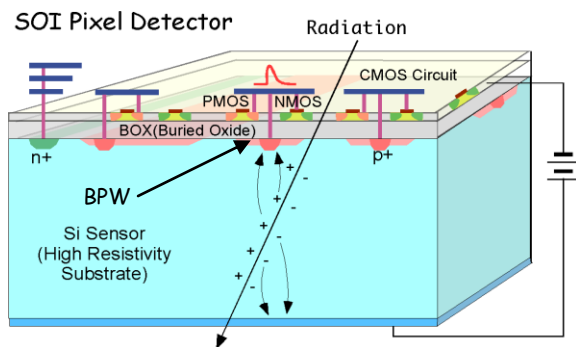
Silicon-On-Insulator (SOI) technology offers a possibility to develop high granularity and thin monolithic pixel detectors. In SOI bonded wafers, the bottom layer is high-resistivity Si and works as a radiation sensor, and CMOS circuits are implemented in the top low-resistivity Si layer, with both layers being separated by an oxide deposition. With this technology complex CMOS circuits can be implemented in each pixel, so that intelligent data handling becomes possible. The technology has the advantages of smaller parasitic capacitances, high speed circuitry and low power consumption as compared to bulk CMOS process.

The monolithic CMOS SOI pixel detector is developed for use in the Belle II experiment at S-KEKB collider and for future applications at ILC or LHC. Such detector is photo-sensitive and can also be used for imaging in outer space experiments and medical applications. R&D is pursued within the SOIPIX Collaboration. The 0.2 μm CMOS Fully-Depleted SOI process of OKI Semiconductor Co. Ltd is used. Prototyping is done by means of Multi Project Wafers (MPW's) that are submitted to production twice a year. A major issue in the use of the SOI wafer as a radiation sensor, that was identified during prototyping is the back gate effect: the potential applied to the sensor part of the structure affects the transistor characteristics despite both regions being insulated by the BOX layer.
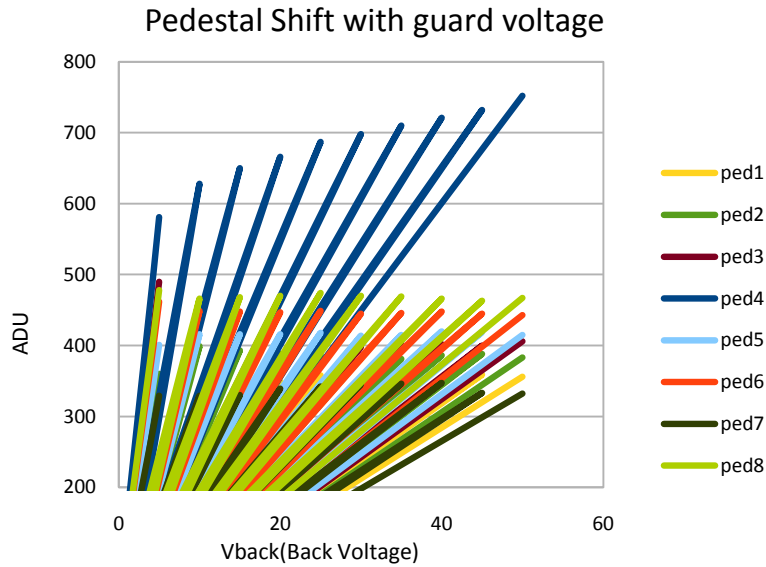
Pedestal Shift with guard voltage

Figure 1: Pedestal Shift versus Back Voltage

INTPIX3 is a pixel detector prototype which I am evaluating. It has a 128x128 array of 20x20μm pixels with integrated basic readout circuit at each sensor. The prototype has been produced to study the method of back gate effect elimination by implanting a buried p-well (BPW) under pixels. The detector is divided into eight 32x64 pixels regions with different BPW shapes and parameters. The I vs. V characteristic of the sensor was obtained to determine the breakdown voltage and the depletion depth. Pedestal shifts in the sensor and I_d vs V_{gs} characteristics of test transistors have been measured for different BPW parameters and the elimination of back-gate effect was confirmed. The fig.1 shows the 4th region without BPW layer, in which pedestals increase with increase of the back voltage. Also the overall increase of ADC values is seen, due to the back gate effect. Other regions show that the back-gate effect is eliminated by introduction of BPW layer.
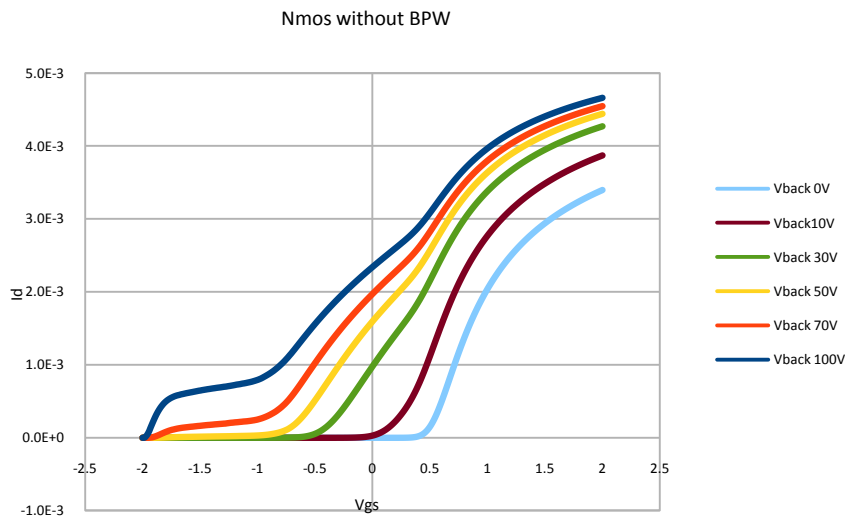
Fig.2: I_d vs. V_{gs} Characteristic of NMOS transistor without BPW layer.

The chip includes, in addition to the detector, a TEG (Test Element Group) containing 13 test transistors with and without BPW implemented, to analyze the back-gate effect at the individual transistor level. I have performed static measurements of sensors and transistors to characterize the technology. A NMOS transistor is used to analyze the back-gate effect, The Fig. 2 shows the I_d Vs. V_{gs} characteristic of NMOS transistor without BPW, where increase in back voltage result in change in threshold voltage. The increase in back voltage effect the top electronics of the sensor which is

nothing but back gate effect. After 50V the transistor are not operational. The Fig. 3 shows the transistor characteristic with BPW. I_g vs V_{gs} curve is not effected by back gate voltage up to 100V This confirms the stabilization of back gate effect by introduction of BPW layer in the design.
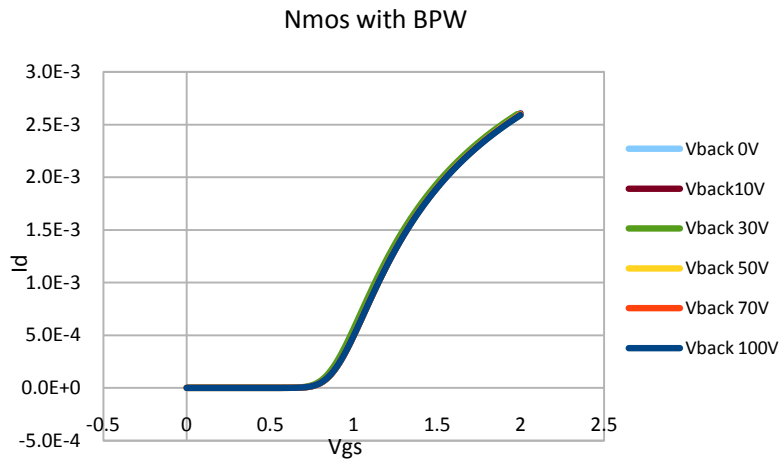
Nmos with BPW

Fig.3: I_d vs. V_{gs} Characteristic of NMOS transistor with BPW layer.

Tests of the sensor have been performed with a red light laser diode and photons from Am-241 source. The Fig. 4 shows that 13.9keV photon energy line is clearly seen at about 60 ADC units in a raw ADC spectrum. Pedestal variations over pixels are studied and clustering algorithm is being developed.
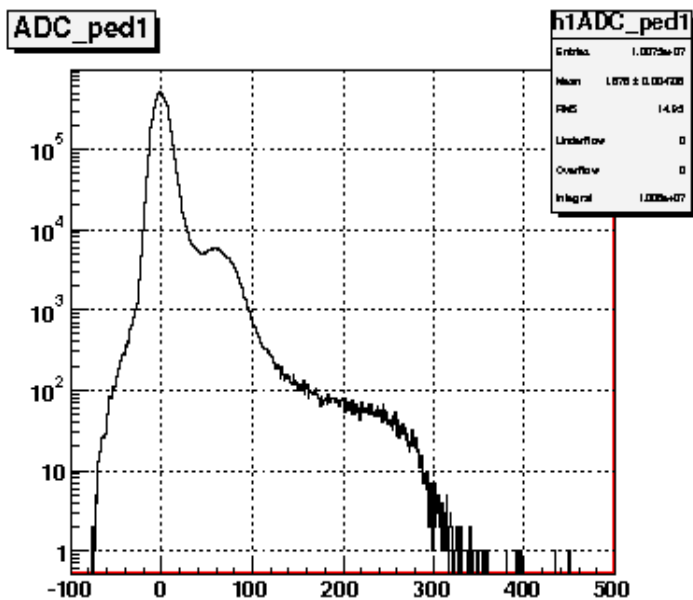

Fig.4: ADC distribution after pedestal substraction for region 6 illuminated with Am-241

Project 11: Frontend Electronics and fast Diamond Detectors

Project Coordinator: Marek Idzik, AGH, Cracow.
Prasoon Ambalathankandy, ESR, WFiIS, AGH, Cracow. Supervisor: Marek Idzik.
Shahinur Rahman, ER, GSI, Darmstadt. Supervisor: Eleni Berdermann

P11 focuses on the development of front-end electronics for particle physics detectors. It includes activities in two centers, namely AGH, Cracow and GSI, Darmstadt. Electronics development at GSI was originally targeted towards electronics for fast diamond detectors. In view of the fact that the ER position could not be filled with adequately educated candidates, the position was redefined as a position for work on diamond detectors. The front-end electronics development task was instead assigned to GSI personnel, where the electronics tests on diamond detectors is and will be realized by the team of the assigned electronics engineer and the MC-Pad ER.

a) Activities at AGH

The report can be broadly classified into three topics.

- ADC Test & Measurements.
- Command decoder module for Multi-channel ADC.
- I^2C interface for readout ASIC's

ADC Testing & Measurement

A detailed test, characterization and verification of the 10 bit ADC was done. This 1st prototype of data converter chip which was developed at WFiIS was thoroughly tested. Also, as the prototype had two slightly different architectures, a study was carried out to choose a suitable architecture for the future Lumi-Multi channel ADC. Advanced laboratory test setup available at WFiIS was judiciously used to carry out the verification. Of the various static and dynamic parameters that were measured, few important results are listed here.

Static parameters:

$-0.5 <$ **DNL** < 0.5

$-1 <$ **INL** < 1

Dynamic parameters:

Signal to noise ratio was found to be at 58.3 dB up to 25 MHz.

Effective number of bits > 9.3 bits.

The ADC measurements are complete and ready to be implemented on the readout system.

Command decoder

The Lumi-Multi channel ADC can have several modes of operation, in order to effectively control the various modes, a command decoder module was developed. The command signal is generated based on the serial word, shown below.

1	0	1	0	1	1	C1	C0	D7	D6	D5	D4	D3	D2	D1	D0

This serial word has a protocol hierarchy, first six bits are the header followed by the command word and lastly eight bits of data set. Command set (C1-C0) has the following data interpretation:

Name	Code	Data interpretation
Config	00	Mode/Test ADC/Low power
Active-ADC	01	Select ADC
DAC-0	10	DAC-0 Value
DAC-1	11	DAC-1 Value

Cadence tools were used to model the decoder in Verilog HDL(Hardware description language). Elaborate verification models were built with self checking test benches to ensure the design functionality, also post synthesis gate level simulations were compared to functional simulations.

I^2C interface for readout ASIC's

This work is aimed at developing new architecture for slow control of readout ASIC's using I^2C protocol as its backbone. Some of the interesting features of the protocol is listed here.

- Two wired bus.
- Slow to medium speed communication.
- Data transfers: Serial, 8 bit oriented, bi-directional.
- Master can operate as transmitter or receiver.

An I^2C Master circuit is being developed in Verilog-HDL that would have the ability to initiate, clock, control and stop a data transfer at appropriate time. Based on these specifications, the circuit is realized by four components.

- Finite state machine
- Logic blocks.
- Clock generator.
- Multiplexers

For verifying the design, we are implementing a FPGA based I^2C Master and will talk to real I^2C device (STCN75-CMOS temperature sensor).

b) Activities at GSI

The fascinating properties of CVD Diamond (CVDD) sensors such as high mobility of both type of charge carriers, radiation hardness, and low dark conductivity provide a detector material, which is suggested to be applied in high intensity heavy-ion beam environments where classical detector devices cannot be operated. In the future 'Facility for Antiproton and Ion Research' (FAIR) experiments radiation-hard materials with large area will be required for a variety of detection applications. Heteroepitaxial quasi-single crystal, CVD diamond grown on 4inch Iridium substrates is investigated as an alternative to homoepitaxial scCVDD, which with actual technologies can have only small dimension.

However, images of the DoI crystal structure revealed a lot of dislocations in the bulk material. The first intriguing feature (not well understood at present) found was an extremely low dark current. To study the conductivity of diamond-on-Iridium detectors, dark current vs voltage (*I-V*) characteristics at higher temperatures have been investigated.
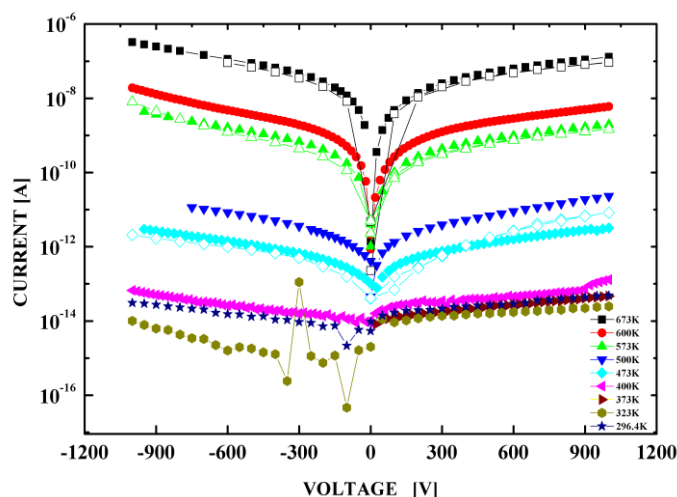

Fig.1 Dark current vs voltage (I-V) characteristics of early DoI (#549a, 230μm) at higher temperatures (from room temperatures to 677K). The solid and open data points correspond two different kind of metallization, Ti-Pt-Au (both side) and Al (one side)/Ti-Pt-Au (other side) respectively on DoI.

Early results showed the dominant conduction mechanism to be electrode-limited conduction, e.g. Schottky emission (*SE*), while we were expecting bulk-limited conduction, i.e. Poole-Frenkel (*P-F*) or space charge limited conduction (*SCLC*) conduction. The Schottky barrier was estimated to Δ_b = 1.72±0.0032eV and the activation energy evaluated to E^{ac} = 1.53±0.002eV. This value is in the range of the activation energy of single-substitutional nitrogen (E^{ac} ~ 1.7eV). Currently, systematic investigations of the dark conductivity of all available CVD diamond materials (scCVDD, pcCVDD and recent DoI samples) are ongoing. From cross-polarizer microscopy, where dislocations and defects in the bulk become visible, it is also clear why the charge collection efficiency (CCE) of old DoI samples was measured so low (CCE ~ 12%): it was due to defective bulk diamond.

In addition to the defective crystal structure, it has turned out that both the signal shape and consequently also the CCE were not well processed by the available front-end electronics (FEE). For

these first studies we used the single-channel diamond broadband amplifiers (DBA-II) developed at GSI for heavy-ion detection, which had a bandwidth of 2.3 GHz and an input impedance of 50Ω.
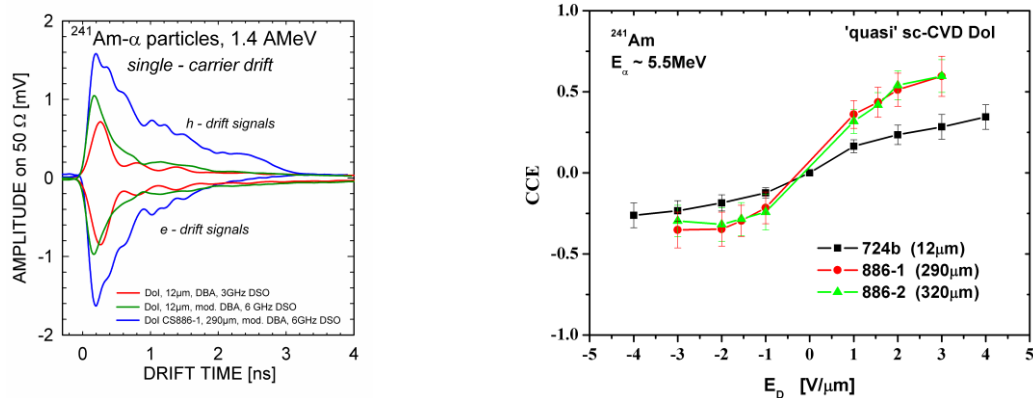

Fig.2. (a) Broadband signals of different DoI samples (#724b,886-1,2)with DBA-II and modiDBA-II. (b) Charge collection efficiency (CCE) as a function of electric field for various DoI detectors with modiDBA-II.

We observed signals showing a dumped oscillation (Fig.2a, red curve) most probably due to the limited bandwidth of the amplifier in conjunction with the 50Ω impedance; hence, we modified the DBA-II for higher bandwidth (3.4 GHz) keeping currently for technical reasons the same input impedance. With this modified DBA-II again the same measurements were performed on the same sample and we noticed that the signal showed a better shape (green curve) and the CCE increased to almost ~ 40% (blue curve). However, recently we received better DoI films (886-1, 2) for which a CCE ≈ 60% has been obtained (Fig.2b). Note that the modified DBA-II is still not the best amplifier solution. Simulations have shown that ballistic deficits dominate the results and this is mainly due to the 50Ω impedance. Future designs of DBA-like amplifiers, are currently investigated in which this present disadvantage will be corrected.
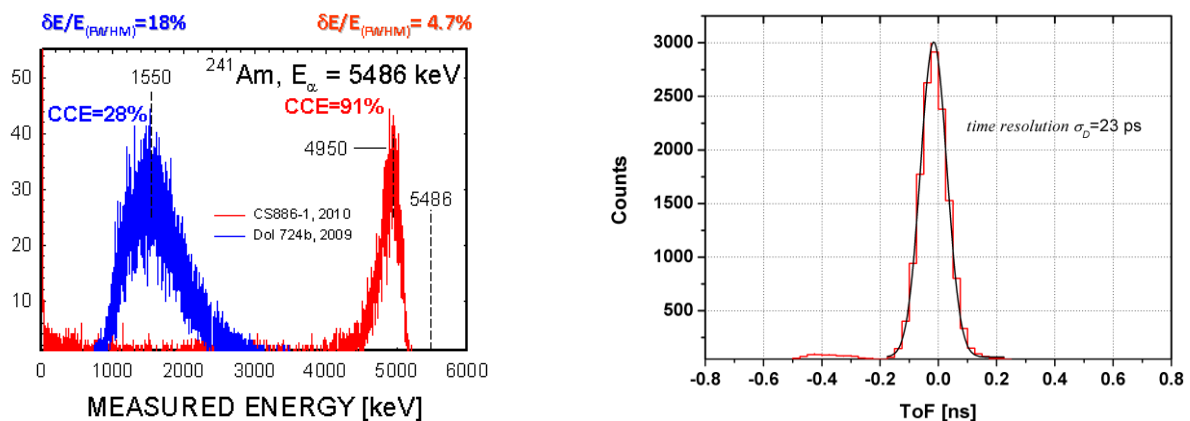
Fig.3. (a) Collected charge spectra obtained from DoI sensors (early sample of 12µm and recent DoI of 290µm), (b) Time of flight (ToF) measurement with recent DoI samples of 290µm and 320µm in the 40Ar 200AMeV beam at GSI.

The precise characterization of the CCE and of the energy resolution δE/E is usually performed under vacuum conditions using high-resolution charge sensitive spectroscopy electronics. For laboratory tests ^{241}Am sources are used to investigate the pulse height resolution of the DoI detectors. The α-signals are amplified with CSTA2 amplifiers developed at the Technical University of Darmstadt and shaped with ORTEC shaping amplifiers using 1µs shaping time. The spectra are recorded with peak-

sensing 13 bit Silena ADC's. An □-resolution of ΔE/E = 18% (FWHM) was found for the early DoI sample of 12□m thickness (#724b), while for the recent sensors of 290□ μm (#886-1) and 320 μm (#886-2) thickness, respectively, values ΔE/E ≥ 4% (FWHM) were measured (Fig.3a). This dramatic improvement is clearly due to the significantly improved growth processes of the DoI material. In order to evaluate the time resolution, the two recent DoI samples were placed perpendicular to an [40]Ar beam of 200 MeAV, mounted in a stack in a distance of 27.2 mm to each other. Fig. 3b shows the measured time-of-flight (ToF) spectrum, which shows a □-width of 48 ps. Assuming equal contribution from each sample, the intrinsic time resolution of the sensors is estimated to $\sigma_i \approx 23$ ps.

Concluding: The electrical characteristics of DoI detectors are improving with respect to the material properties. The following approach has been elaborated for the new generation of single-channel broadband amplifiers for the characterization of the ultra-fast DoI detectors: low noise, low capacitance, amplifiers of a BW>3GHz and an input impedance R > 50Ω have to be developed. In addition, encouraging results have been obtained with a special BB ASIC for diamond detectors (PADI-4) tested for the first time with single-crystal CVDD diamond sensors in the same [40]Ar beam test. The latest developments are the first steps towards large-area diamond-strip sensors for tracking and ToF in FAIR experiments.

Project 12: Optimization of Monte Carlo Tools and Comparison with Benchmark Data

Project Coordinator: Stefano Miscetti, INFN Frascati

Mary Tsagri, ESR, CERN. Supervisor: John Apostolakis

Filimon Roukoutakis, ER, INFN Frascati, Supervisor : Stefano Miscetti

Detailed simulation of gaseous detectors and lead/scintillating fibers (Scifi) calorimeters of different structures using Monte Carlo tools (FLUKA[1], Geant4[2]) is relevant to evaluate and improve their energy response and sensitivity to neutrons. The first study will determine the impact of the expected strong neutron background on the energy deposition measured in chambers, which is a background and potential limitation of the performance of gaseous detectors in HEP experiments. The second study is mainly motivated from the fact that the KLONE collaboration [ref 5-6], has measured an increase of neutron detection efficiency in heterogeneous calorimeters (lead/scifi) with respect to simple scintillation counters with an equivalent quantity of active material. Results critically depend on the lead/fiber volume ratio so that an accurate simulation is needed to understand the physics mechanism and to improve the response. The studies are carried out by one ESR at CERN, Mary Tsagri, which mainly contributes on the gaseous detector and one ER at LNF, Filimon Roukoutakis, which is instead dedicated to calorimetry. The first simulation is in a more advanced state since it has started in time with the project in December 2009 and is shown here in two sections: a) the Geant4 validation for neutron cross section in gases and b) the evaluation of the energy deposition in gasses. The second part is slightly behind since it only in its starting phase (April 2010). This will be reported in the final section as: c) simulation strategies for lead-scintillating fiber calorimeters.

A) Validation of neutron cross sections of gaseous detectors

The modeling accuracy of neutron interactions in Geant4 is being validated using published benchmark and test beam data. The major work consisted in validating the Geant4 neutron interaction cross-sections for key gases such as Helium, Argon, Krypton, Xenon, and quenchers as Hydrogen, Oxygen and Carbon, which are widely used in HEP gaseous detectors. This aims to source of cross sections for these elements, and identify areas for improvement using recent data libraries. Moreover, the creation of a prototype interface between Geant4 and Garfield[3] has also been carried out to model the effect of neutrons on the energy deposition in gas chambers.

The interaction of neutrons with the detector atomic nuclei relies on measurements which limit the simulation accuracy. A first task was to trace back the origin of the used neutron cross-sections by Geant4, and identify which must be updated from more recent libraries. The validation used benchmark data from various neutron Libraries, using recent as well as older evaluations.

Data Libraries used in this work:

ENDF/B-VII.0 & ENDF/B-VI.8: Evaluated Nuclear Data File (December 2006 and 2001, respectively)

JEF-2.2 :   Joint Evaluated File (January 1997)

JEFF-3.0 :   Joint Evaluated Fission and Fusion, "...this library superseded JEF-2.2..." (April 2002)

JEFF-3.1 :   "...this library superseded JEFF-3.0..." (May 2005)

JEFF-3.0/A :   Neutron Activation File

JENDL-3.3 :   Japanese Evaluated Nuclear Data Library (2002)

Geant4 physics choice and corresponding neutron cross sections:

The neutron cross sections which were tested are those used in two physics lists: QGSP_BERT (=QGSP BERTINI) production by the LHC and other experiments and QGSP_BERT_HP (=QGSP BERTINI HIGH PRECISION), which is recommended for HEP uses where the detailed modeling of neutrons below a few MeV is required.

QGSP is the basic physics list applying the quark gluon string model for high-energy interactions of p, n, pi, K and nuclei. QSGSP_BERT is like QGSP, but uses Geant4 Bertini cascade for primary p, n, pi and K below about 10 GeV. QGSP_BERT_HP list is similar to QGSP_BERT except that it uses the data-driven HP ("high-precision") neutron package to transport neutrons below 20 MeV in place of the Bertini model. It includes cross-sections and interactions down to thermal energies.

i. Validation and Results of Geant4 performance

In Fig.1 we compare the cross section in Geant4 for Argon with the data libraries. Results are also available for: Helium, Oxygen, Xenon, Krypton, Hydrogen and Carbon. The summary of this work is reported in Table 1.

ii.   Simulation with Quencher Gases

The high multiplicity of particles/event and the high rate of LHC collisions translates to a high neutron background in the detectors with an energy spectrum up to ~ 10 MeV. We therefore started by simulating mono chromatic neutrons of energies in the range 1--10 MeV. Elastic recoils of heavy nuclei, like Argon, deposit energy below 10--100 keV, which however increases for decreasing atomic number A. Indeed, the minimum energy (E') of an elastically scattered neutron, occurs for a head-on collision, $(E'/E)min=[(A-1)/(A+1)]^2$. For A=1 (neutron on Hydrogen), the neutron can release all its energy to the struck proton. The case of Hydrogen is therefore the most important since it is part of the chemical composition of various quenchers, contributing to ~5--10% of the total gas composition.
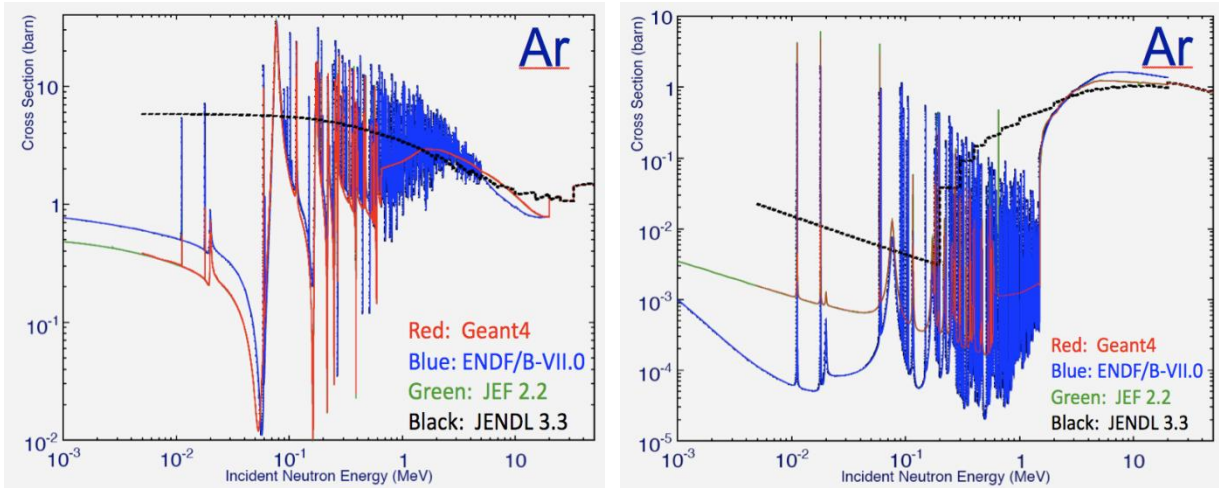
Figure 1. Comparison between Geant4 and the "old" libraries over all energy regions. Large discrepancies appear with the "new" libraries. For the case of Argon, G4NDL uses JEF 2.2 / JEFF 3.0.

Energy Region	< 1 MeV	1 - 10 MeV	> 10 MeV
Argon			
Elastic	JEF 2.2	JEF 2.2	JEF 2.2
Non-Elastic	JEF 2.2	JEF 2.2	JEF 2.2
Helium			
Elastic	ENDF / JEFF	ENDF / JEFF	ENDF / JEFF
Non-Elastic	ENDF / JEFF	ENDF / JEFF	ENDF / JEFF
Oxygen			
Elastic	ENDF / JEFF	ENDF / JEFF	ENDF / JEFF
Non-Elastic	No agreement	ENDF	ENDF
Xenon			
Elastic	JEFF 3.1	JEFF 3.1	JEFF 3.1
Non-Elastic	ENDF / JEFF	ENDF / JEFF	ENDF / JEFF
Krypton	Bromine's cross-sections are used instead.		
Elastic			
Non-Elastic			
Hydrogen			
Elastic	ENDF/JEFF/JENDL	ENDF/JEFF/JENDL	ENDF/JEFF/JENDL
Non-Elastic	ENDF/JEFF/JENDL	ENDF/JEFF/JENDL	ENDF/JEFF/JENDL
Carbon			
Elastic	ENDF/JEFF/JENDL	ENDF/JEFF/JENDL	ENDF/JEFF/JENDL
Non-Elastic	JENDL 3.3	JENDL 3.3	JENDL 3.3

Tab.1 Neutron libraries tested in Geant4 for different gases and different neutron energy regimes.

Thus, the impact of the quencher is not at all negligible, since a recoiling proton can take a large fraction of the neutron energy. Such recoiling protons will deposit their energy as relatively long tracks and they cannot be suppressed easily, a dedicated reconstruction analysis is needed. This work allows quantifying the implications of hydrogen compositions like, for instance, the quencher gas CH_4.

iii. Conclusions

This work makes future Geant4 updates easier to implement. Throughout this work we have focused on typical gas compositions used for chambers in HEP experiments. We have identified that for Ar,

Xe, Kr, H, C and O Current Geant4 mostly follows JEF 2.2. Neutron cross-sections in the G4NDL format have been created using recent libraries that have been provided by the group of D. Cano Ott (CIEMAT). Revisions have been prepared in the Geant4 code to handle additional data formats , and their release is foreseen in the near future.

B) Evaluation of energy deposition in gasses

The mechanism by which neutrons deposit energy in gases is via collisions which produce electrons or gammas or by transferring energy to an atom of molecule of the gas atom. To identify the precision possible for this energy deposition a study is undertaken of the relative strengths of the modeling of energy deposition of charged particles in Geant4 and competing codes which model detailed effects in gases.

i. Simulation of energy deposition at the atomic level

The Bethe-Bloch formula provides the energy deposition of charged particles propagating in matter. This includes the various components dominating the different charged particle velocity regions. The standard Electromagnetic (EM) models in Geant4 code do not emit low energy photons and delta ray in the sub-keV range, modeling this energy as local deposition. The low-energy models in Geant4 and other codes, such as HEED[4], have refined modeling of shell effects and include de-excitation, fluorescence, Auger electrons and sub-keV δ-rays. A comparison has been made between Geant4 and HEED.

i. Validation of energy loss distribution for minimum ionizing particles

While validating the overall performance of the Geant4 code for ionization, the energy loss distribution for 500 MeV electrons and muons in 1.5 cm of Argon has shown an unexpected spectral shape (see Fig. 2) with a second bump appearing on the higher energy side of the main peak. Such secondary peak has been investigated in depth to understand its origin. Under the same conditions, a simulation run was performed also with FLUKA, and provided quite identical results. Later, FLUKA experts produced a reconstructed spectral shape with an evident second peak, to which they assigned a clear physical meaning. The collision of the primary electron with an electron on the K-shell of the Argon atom, which has a binding energy of 3 .2 keV, well comparable with the most probable energy loss in a 1.5 cm Argon layer (~ 3 keV), provides a release of this binding energy to the gas. This could proceed either through the emission of a fluorescence photon or, with much higher probability, via an Auger electron. Finally, we have discovered that the bump in Geant4 is just an artifact due to limitation in the simulation of fluctuation. An improved fluctuation model is prepared and will be included in the next release.
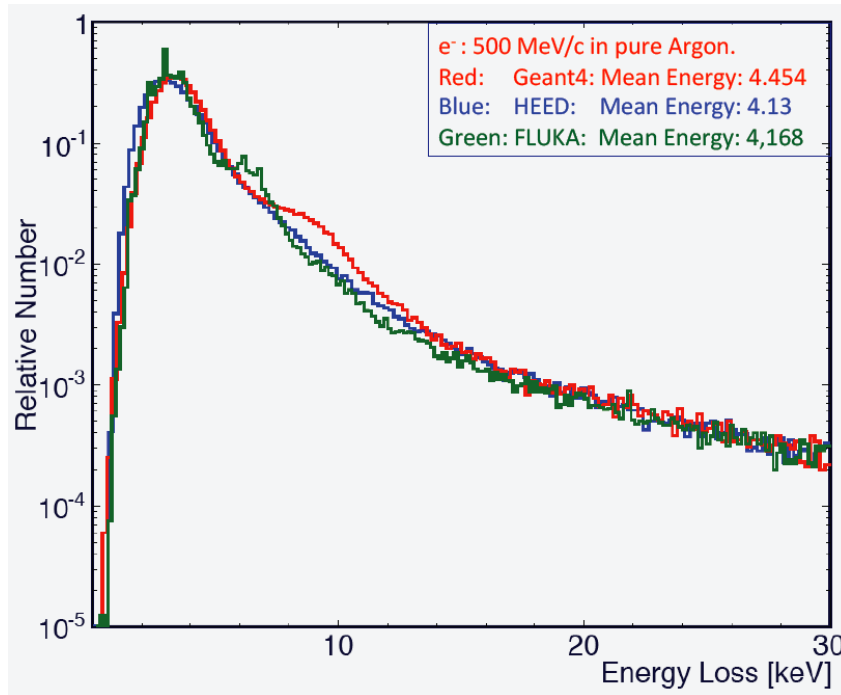
Figure 2. Ionization energy loss produced by 500 MeV/c electrons in 1.5 cm pure Argon. Comparison between Geant4, HEED and FLUKA codes.

C) Simulation strategies for lead-scintillating fiber calorimeters

The requirement for a detailed simulation of several lead/scintillating fiber calorimeter geometries using both Geant4 and Fluka led to the choice of utilizing Virtual Monte Carlo (VMC) [7] as a framework. VMC has been developed by the ALICE-LHC collaboration and it is also used by other collaborations such as PANDA and ILC-D. It is also currently part of the ROOT Data Analysis Framework [8]. VMC provides a consistent detector description between Geant4 and Fluka, by using the ROOT geometric modeler. In addition, since VMC has been modeled after Geant3, we have the possibility to use also this simulation code. During the first period of the project, the existing FORTRAN code for the Geant3 simulation of an E/M calorimeter prototype, from KLOE collaboration, has been studied thus allowing us to extract the Geant3 geometry and to create the geometry in ROOT format.

 At the moment, the VMC application is working as expected and its implementation is very close to the original design. We are currently working on more detail on the calorimeter geometries. Currently the geometries are described as C++ functions where function arguments describe the key values of the geometry and materials. The consistency of the input values is checked at runtime inside the function itself, proving already the superior approach of using a full programming language as C++ for detector description with respect to the classical approach of using dedicated input like in the case of Fluka or an XML schema. We currently have two such functions, one using the original KLOE calorimeter geometry and the other describing the "SpaCal" geometry. The two geometries differ in the cell structure with respect to the positioning of the scintillating fibers inside the absorber cell. Both geometries exist in one "coarse" version and two "detailed" versions, following the original Geant3 implementation of the simulation. This can be selected at runtime. The "coarse" geometry assumes that the fiber coincides with its plastic core, while the detailed geometries assume that there is also fiber cladding and glue attached.

Part of the simulation framework is the primary particle generator. The framework that we have developed allows the runtime plugging-in of a user-provided generator following a very simple interface. For our specific use-case of the calorimeter simulation, three such generators have been developed. The first one is simple fixed particle "gun" which generates a specific type of particle with fixed momentum and origin. The second one is a parameterized generator that can generate a specific particle whose momentum and/or position vector components follow a histogram distribution. The third generator follows the same logic that was used to simulate with Fluka the calorimeter that was tested by the KLOnE collaboration in TSL, Uppsala in 2007. It generates neutrons in a fixed position and with a fixed direction with random kinetic energy following a provided energy distribution. We currently have three different distributions filed as histograms corresponding to the three different energies used during the test-beam.

We are now able to routinely run simulations with both the mentioned geometries, varying the geometrical parameters as well as the detector materials. We have tried to change the physics simulation parameters of both Geant3 and Geant4 and noticed a significant difference in the energy deposited by varying the Geant3 energy loss models. A factor of two energy resolution with respect to the benchmark numbers from KLOE was found when activating the default energy loss mechanism, "Continuous energy loss without generation of δ-rays and full Landau-Vavilov-Gauss fluctuations", a reasonable response was instead found with model "Continuous energy loss with generation of δ-rays above DCUTE (common /GCUTS/) and restricted Landau fluctuations below DCUTE". Validation of the VMC application has been done with a first analysis of energy resolution dependence of the calorimeter when exposed to E/M showers initiated by e or gamma of different energies. In Fig. 3, a comparison between Geant3, Geant4 and the value of sampling fluctuation from KLOE measurements is shown.
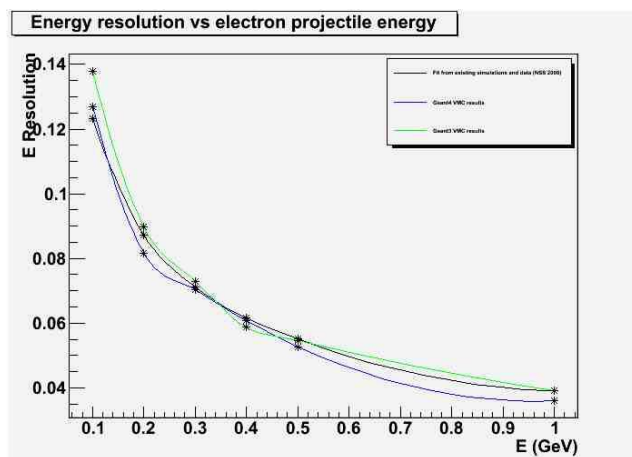

Figure 3. Energy resolution as a function of electron energy for Geant3/Geant4 and KLOE measurements.

We are now working in implementing the treatment for optical response. In Geant4 case, we are able to observe scintillation photons produced according to the yield expected from the provided scintillation parameters. Geant3 does not have scintillation mechanism but we plan to implement one in VMC by back-porting the Geant4 code accordingly. This will allow a deeper comparison between Geant3 and Geant4 optical transport properties since Geant3 has optical photon transport capabilities itself.

Conclusions and plans

The proof of concept for a generic VMC application as a turn-key detector simulation solution has been achieved. We are now validating the physics results against benchmark E/M data. A more complete view will be available as soon as the complete simulation chain, up to the PMT response is simulated. We also plan to consolidate the application and try it with different geometries to identify additional needs. Due to licensing issues with Fluka since March 2010, it was not possible to use Fluka VMC for comparison. The Fluka collaboration has recently announced that they plan to support Fluka VMC again before the spring of 2011. This will allow us an easy comparison with the results obtained during the 2008 test beam in Uppsala.

References

[1] Battistoni, G., Cerutti, F., Fasso, A. , Ferrari, A. , Muraro, S. and Ranft, J. and Roesler, S. and Sala, P.R., The FLUKA code: description and benchmarking p31-49, in Hadronic Shower Simulition Workshop, Edited by Albrow, M. & Raja, R., American Institute of Physics Conference Series, Vol. 896 (2007)

[2] Geant4: a simulation toolkit, (Geant4 Collaboration), Agostinelli, S. et. al. Nucl. Inst. Meth. A506, pp. 250-303, 2003

[3] Garfield, recent developments, Veenhof, R., Nucl. Inst. Meth. A419, pp. 726-730, (1998).

[4] Modeling of ionization produced by fast charged particles in gases, Smirnov, I.B., Nucl. Inst. Meth.A554, pp. 474 – 493, (2005).

[5] NIM A 581 (2007), 368-372

[6] NIM A doi:10.1016/j.nima.2009.09.104, NIM A doi: `10.106/j.nima.2010.10.094`

[7] http://root.cern.ch/drupal/content/vmc

[8] http://root.cern.ch/drupal/